USING GROUND-PENETRATING RADAR AND CAPACITIVELY COUPLED RESISTIVITY TO INVESTIGATE 3-D FLUVIAL ARCHITECTURE AND GRAIN-SIZE DISTRIBUTION OF A GRAVEL FLOODPLAIN IN NORTHEAST BRITISH COLUMBIA, CANADA

ADRIAN S. HICKIN,[1] BENJAMIN KERR,[1] THOMAS E. BARCHYN,[2] AND ROGER C. PAULEN[3]

[1]British Columbia Ministry of Energy, Mines, and Petroleum Resources 1810 Blanshard Street, Victoria, British Columbia, V8W 9N3, Canada
[2]Department of Geography, University of Lethbridge, C866, University Hall, 4401 University Drive, Lethbridge, Alberta, T1K 3M4, Canada
[3]Geological Survey of Canada, 601 Booth Street, Ottawa, Ontario, K1A 0E8, Canada
e-mail: adrian.hickin@gov.bc.ca

ABSTRACT: This study combines ground-penetrating radar (GPR) and capacitively coupled resistivity (CCR) for geophysical architecture-analysis of a bar platform and channel bend on the floodplain of a poorly organized wandering gravel-bed river. An important objective of fluvial architectural analysis is linking fluvial style with preserved subsurface sedimentology. However, architectural analysis relies on opportunistic outcrops with locations or orientations that may not provide appropriate data. GPR is a well-established geophysical method that images reflections interpreted to represent bed geometry and bounding surfaces and is therefore ideal for imaging fluvial architecture. Unfortunately, grain-size information, which is integral to architectural classification, is more elusive using GPR. Resistivity data can be used as a proxy for sediment grain size. When GPR and CCR are combined they offer an effective tool for geophysical fluvial architectural analysis.

Five trenches provided direct observation of the subsurface sedimentology and are used to calibrate the two geophysical methods. Eight radar facies and one radar element are classified from the GPR survey and grouped into four categories: horizontal and subhorizontal, laterally continuous reflections (Group 1), clinoform reflections (Group 2), discontinuous reflections (Group 3), and concave-up elements (Group 4). The 2-D resistivity data are combined in a GIS to establish a 3-D resistivity model for the upper 5 m of the floodplain. Resistivity values correlate well with grain size and are categorized into fine-grained (< 400 ohm-m), sand-size (400 to 800 ohm-m) and gravel-sized (> 800 ohm-m) sediments. In general, resistivity values indicate coarse sediment in the bar platform and sand to fine-grained material in the main channel and subordinate depressions. Resistivity profiles were extracted from the 3-D model along the GPR lines so that resistivity values could be directly compared to radar facies. The shape and spread of the resistivity distributions provide dominant grain size as well as an indication of sediment sorting for individual radar facies. In some cases, the same radar facies is associated with markedly different grain sizes, indicating different architectural elements (i.e., horizontally bedded gravel verses horizontally bedded sand or fine-grained sediment). This demonstrates the utility of combining GPR and CCR, insomuch as radar architecture alone is not diagnostic of fluvial architectural elements.

In this case study, the bar platform and channel have a planform that might suggest a meandering fluvial style. However, GPR-CCR results indicate that the dominant depositional process across the bar platform was vertical accretion of gravel sheets, an architecture more consistent with a wandering gravel-bed fluvial style. Lateral migration was limited to the outer downstream margin of the platform, a location dominated by a mix of sand and gravel. Coarse gravel likely occupies the base of the main channel, with fine-grained sediment contributing to the remainder of the channel fill. A four-phase history is presented where the initial phase of development involves vertical accretion and migration of stacked gravel-sheets during floods, forming the core of the bar platform. After flooding subsides and the interior bar emerges, the channel becomes established and lateral migration becomes the dominant depositional process. The evolution concludes with avulsion and eventual abandonment of the channel.

INTRODUCTION

This case study combines ground-penetrating radar (GPR) with capacitively coupled resistivity (CCR) to examine the subsurface architectural structure and grain-size distribution of several discrete morphostratigraphic units on a natural floodplain. Brierley (1991) uses the term morphostratigraphic unit to describe floodplain surface features, and differentiates individual units by their 3-D surface geometry in association with their sedimentary characteristics (e.g., bar platforms and

channels). Linking fluvial morphostratigraphic units with preserved subsurface sedimentology from vertical profiles has been criticized in the past (Allen 1983; Bridge 1985; Brierley 1989). Miall (1996) addressed this criticism through architectural-element analysis, a method that involves mapping the 2-D and 3-D character of fluvial deposits. Sediment architecture (i.e., bed and bounding-surface geometry) and grain size are integral to Miall's method, in that these characteristics define the classification terminology (e.g., gravel bars and bedforms—GB, sandy bedforms—SB, laminated sand sheet—LS). Any indirect methodology
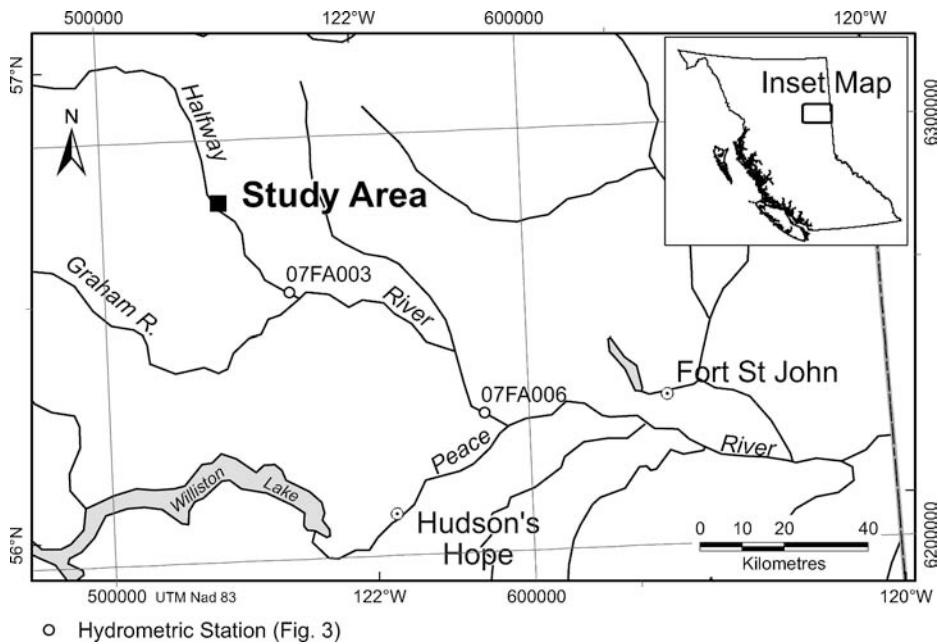
Fig. 1.—The study area is located at the Scobie Ranch on the Halfway River floodplain in northeast British Columbia.

developed for fluvial-architecture analysis needs to address both of these fundamental parameters. The methodology presented in this study utilizes radar for imaging the subsurface architecture and CCR data as a proxy for sediment grain size.

Direct observations of sedimentary architecture and distribution of lithofacies within fluvial deposits is often difficult, relying on opportunistic natural exposures or destructive investigative techniques such as trenching or excavation (e.g., commercial sand and gravel operations). Consequently, there is a deficiency of work linking surface processes to the preserved deposits. The application of high-resolution geophysical surveys has enabled considerable advancement in addressing this deficiency. Mesoscale and macroscale fluvial architecture (Miall 1996) has been routinely imaged by GPR (e.g., Gawthorpe et al. 1993; Huggenberger 1993; Stephens 1994; Beres et al. 1995; Bridge et al. 1995; Bristow 1995; Olsen and Andreasen 1995; Leclerc and Hickin 1997; Roberts, et al. 1997; Bridge et al. 1998; Beres et al. 1999; Vandenberghe and van Overmeeren 1999; Neal 2004; Wooldridge and Hickin 2005; Bersezio et al. 2007; Kostic and Aigner 2007, Mumpy et al. 2007). GPR measures the travel time of electromagnetic waves that reflect off horizons of contrasting dielectric properties (Davis and Annan 1989) yielding vertical profiles that depict architectural features (Jol and Smith 1991).

Although GPR investigations have made significant contributions to the understanding of sedimentary architecture, without considerable data processing (Moysey et al. 2006) GPR is unable to effectively resolve sediment grain size. This information is critical in architectural analysis and the development of 3-D facies models (Miall 1985; Miall 1996). Ground-based resistivity is a technique that can partially fulfill this role. Resistivity surveys inject current into the ground using two current electrodes. The difference in voltage between two voltage electrodes is subsequently measured, from which the apparent resistivity can be calculated. The effectiveness of a survey is dependent on geological complexity, ground conditions, method (e.g., electrical resistivity, capacitively coupled resistivity, or electromagnetic induction), and electrode configuration. The target depth of investigation can be manipulated by varying the spacing of the transmitter and receiver electrodes. With multiple receiver electrodes set at various distances from the transmitter electrodes, a vertical geometric model (i.e., a pseudosection) of the electrical structure of the subsurface can be produced (Edwards 1977). The electrical structure of the substrate is closely related

to porosity, pore fluids (e.g., content, composition, and temperature), grain size, and mineralogy (Archie 1942; Best et al. 2005). In general, clay and silt tend to be more conductive (low resistivity) whereas sand and gravel are more resistive (Reynolds 1987; Reynolds 1997; Best et al. 2006). Traditional resistivity data are acquired through inductively coupled techniques where electrodes are hammered into the ground. Modern surveys generally involve many electrodes controlled from a single location, which significantly increases the speed of data collection. However, the process still requires the electrodes to be manually placed, resulting in time-consuming and labor-intensive surveys. Alternatively, capacitively coupled resistivity (CCR) surveys use electric dipoles that are not grounded, but towed across a survey area. The dipole transmitter capacitively injects current into the ground and the dipole receiver detects the voltage, again through capacitive coupling. This technology enables the rapid collection of shallow, high-resolution data over large areas in a relatively short period of time. The depth of investigation in CCR is more limited than conventional resistivity because there is a larger skin depth effect associated with the relatively high frequency (16 kHz) at which CCS operates. Skin depth is the depth within a conductor (in this case the ground) at which the amplitude of a time-varying electric or magnetic field is 37% of the amplitude of the electric or magnetic field at the surface of the conductor. CCR is further limited by the distance over which the dipole receiver can detect the signal from the dipole transmitter.

STUDY AREA

This study was conducted at Scobie Ranch, on the floodplain of Halfway River in northeastern British Columbia, Canada. Halfway River originates in the Rocky Mountains and flows south to Peace River (Fig. 1). In this area, Halfway River is best described as a poorly organized wandering gravel-bed river, as defined by Church (1983) and Nanson and Knighton (1996) (Fig. 2). The floodplain has been cleared for agricultural activities, and the open fields allow an unimpeded survey. Thus, it is an ideal site for imaging the radar architecture and testing the utility of CCR for determining 3-D grain-size distribution.

Two hydrometric-station records are available from Environment Canada for the lower Halfway River. One station is located upstream (north) of Graham River, the other downstream (south) of the confluence of the Graham, near Peace River (Fig. 1). The northern station
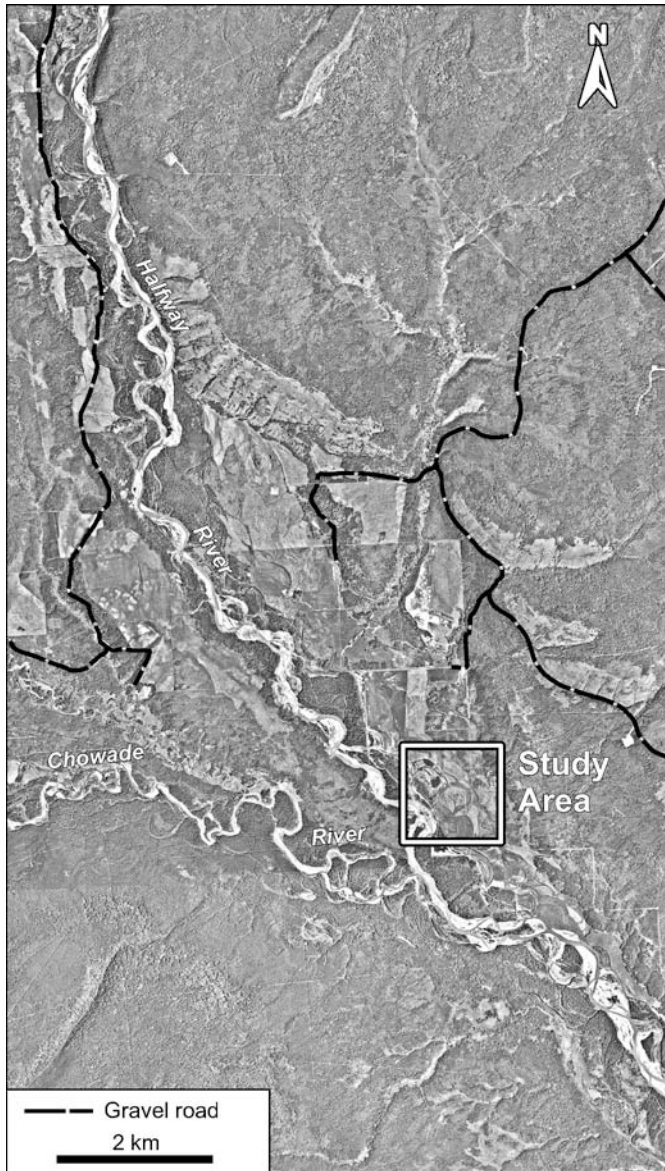
Fig. 2.—This reach of the Halfway River is best described as a poorly organized wandering gravel-bed river. The study area is outlined.

(07FA003) has data between 1977 and 1995 but is currently inactive; the southern station (07FA006) has a record that includes data from 1984 to 2005 (Fig. 3). The records show similar trends, although the southern station has higher discharges with the addition of Graham River to the Halfway River catchment. Peak annual discharge is driven by snowmelt during the spring and early summer. The records indicate that flood events are crudely cyclical with relatively high mean discharge (averaged over a month) occurring every 5–6 years.

A series of five sequential aerial photographs (1963, 1978, 1987, 1992, and 1999) yield a 37-year record of change in the Halfway River planform near the study area (Fig. 4). Although the features studied here have remained stable for this period, the bars and channels developed since 1963 represent analogues for morphostratigraphic units preserved on the floodplain.

The main channel has distinctly sinuous meanders, and lateral bars are present. However, the many semipermanent vegetated and nonvegetated bars and islands with secondary channels are more typical of wandering

gravel-bed rivers (Church 1983; Carson 1984a; Carson 1984b; Carson 1984c; Schumm 1985; Desloges and Church 1987; Brierley and Hickin 1991; Nanson and Knighton 1996). Main channel migration tends to be variable and characterized by phases of rapid shifting. As the dominant channel becomes choked with sediment, it avulses and occupies new or subordinate channels (presumably during flood), abandoning the former thalweg (Fig. 4).

The Halfway River planform is indicative of a system dominated by bed-load transport (Schumm 1985). Evidence of sheeted gravel transport is preserved on bar tops (bar 2, Figs. 4, 5). Sheets of gravel with prograding slip-faces were observed and left in place when transport capacity of the stream decreased during waning flow (Ferguson and Werritty 1983). Abundant channels dissect bar 2, and channel bottoms contain imbricated cobble gravel. In places the channels have been infilled with fine-grained organic mud (Fig. 5F).

The focus of the study is a former channel bend and an associated interior bar platform (Fig. 6). The main channel appears to have been an eastward-migrating river bend that eroded into the pre-existing floodplain. The interior bar has two subtle, positive topographic regions and four poorly defined topographic lows that are interpreted as bar platforms and subordinate ridges and swales, respectively. The western platform stands approximately 1.0 m above the eastern platform, separated by a topographic low that is indistinct to the northwest but narrows and deepens to form a channel where it meets the main river bend (between GPR Lines 4 and 5; Fig. 6).

METHODS

The study, conducted in the winter of 2006, consisted of three components: (1) trenching; (2) GPR survey; and (3) CCR survey. Five sites were trenched with an excavator to depths between 3.2 and 4.5 m. Trenches were located near GPR lines on three of the main morphostratigraphic units (Fig. 6). At each location, lithofacies were described and photographed. Bulk samples were collected from the gravel component at four of the trenches. Grain-size analysis was conducted on the samples following procedures outlined by the Canadian Standards Association (ASTM C 136-06). The proportion of oversized clasts (> 75 mm; Modified Unified Classification System for Soils) were estimated in the field and incorporated into the normalized proportions.

The GPR survey was conducted using a Sensors & Softwares pulseEKKO IV GPR system with a 400 V transmitter and 100 MHz antennae. The survey was conducted following procedures and survey design described in Sensors & Software (1996). Antennae were oriented perpendicular to the direction of travel with a fixed separation of 1.0 m and traces collected at 0.5 m intervals. The survey consists of five lines, two of which are oriented southwest–northeast (Lines 1 and 2) and three lines are oriented approximately northwest–southeast (Lines 3–5), orthogonal to Lines 1 and 2 (Fig. 6). Lines were spatially located with a hand-held global-positioning system (GPS) every 10 to 20 m. A velocity of 0.132 m/ns is used to convert the time scale to a depth scale, estimated from the mean of two common-midpoint surveys (CMP) collected at locations within the interior bar. Processing includes dewowing the saturation signal, applying an automatic gain control (set at 1000) to enhance later arrivals, and applying topographic trace adjustment to account for subtle changes in elevation. Filters were set with trace-to-trace averaging at 4 and down the trace averaging at 7 to enhance the signal-to-noise ratio (Sensors & Software 1996).

Radar facies and element interpretations are based on the principles of radar stratigraphy (Beres and Haeni 1991; Jol and Smith 1991) derived from seismic stratigraphy (Mitchum et al. 1977). Radar facies are defined as mappable 2-D units composed of reflections whose internal reflection configuration, continuity, amplitude, polarity, spacing, and external 2-D geometry differ from adjacent units (Jol and Smith 1991). The resolution
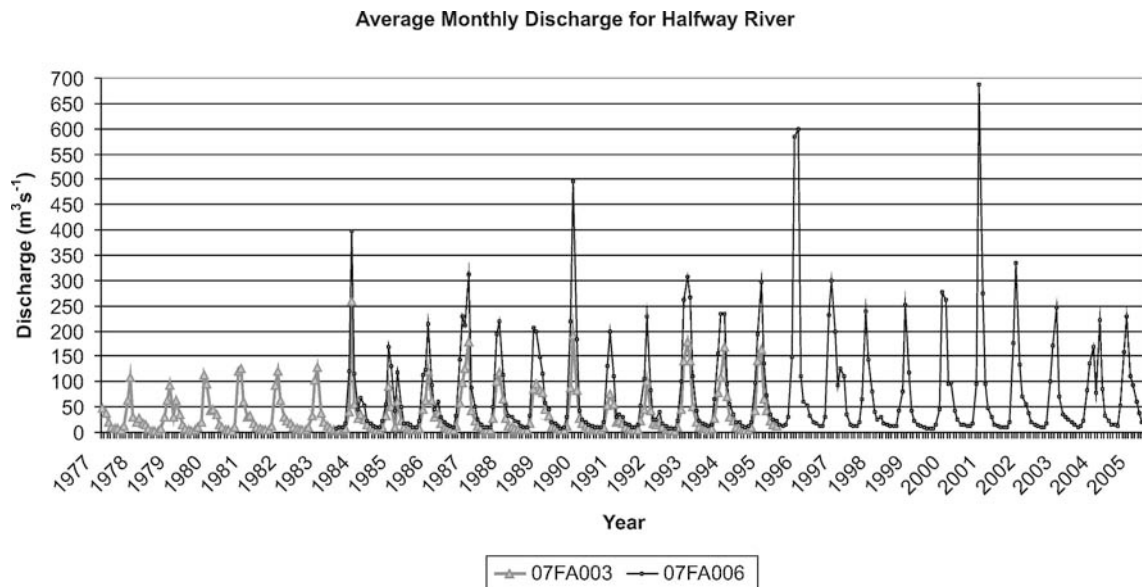
Average Monthly Discharge for Halfway River

F<small>IG</small>. 3.—Two hydrographs show the mean average monthly discharge of the Halfway River. Station 07FA003 is located downstream of the study area but above the confluence of the Graham and Halfway rivers. Station 07FA006 is located below the confluence towards the Peace River (Fig. 1).

of a GPR survey is dependent on the central operating frequency of the antenna. The scale of bedding, bounding surfaces, and the resulting radar facies resolved in a given survey are therefore also dependent on the central operating frequency (Woodward et al. 2003). Closely related radar facies can be combined to form radar elements in much the same way lithofacies combine to form architectural elements (Miall 1978; Miall 1985; Miall 1996). Genetic interpretation of the radar facies for wandering gravel-bed rivers follows Wooldridge and Hickin (2005).

The CCR survey was conducted with an OhmMapper<small>TM</small> instrument configured with five, 5 m dipole receivers and a dipole transmitter with a 5 m rope length, arranged in a dipole–dipole array (Geometrics 2001) (Fig. 7). Readings were collected continuously at 0.5 second intervals, traveling at approximately 6 to 10 km/h with receivers spaced at $n = 1.0$, 1.5, 2.0, 2.5, and 3.0 (n is equal to the dipole length). This resulted in a vertical pseudosection of approximately 5 m depth. Lines were spaced approximately 10 m apart, and positional data were continually acquired with a hand-held GPS. Topographic data from a high-resolution light detection and ranging survey (LiDAR) were incorporated into each line. The raw CCR data were uploaded into Geometric's MagMap2000<small>TM</small> software and individual lines exported in a format compatible with inversion software (RES2DINV<small>TM</small>; Griffiths and Barker 1993; Loke and Barker 1996). Lines were inspected and poor data points removed. RES2DINV<small>TM</small> provides a 2-D resistivity inversion of the subsurface for data obtained from electrical imaging surveys (deGroot-Hedlin and Constable 1990; Griffiths and Barker 1993; Loke and Barker 1996). Robust inversion was chosen because this method enhances sharp boundaries (Claerbout and Muir 1973). A soft user-defined boundary was included at 1.25 m with a boundary weight factor of 50. This enables the inversion software to invoke a sharp boundary near the defined depth, but does not force the boundary if not supported by data. The weight factor reflects the rigor with which the inversion incorporates the boundary (Geotomo Software 2006). With the above configurations, the model generated low-resistivity values in the channels where fine-grained sediments were noted in trenches or at surface. The inversion process was iterative, and parameters were altered systematically until the software generated a geologically reasonable model that was consistent with field observations. Once the parameters were optimized, batch inversions were performed on all lines.

A 3-D resistivity model was generated using Golden Software's Voxler<small>TM</small> (Golden Software 2006) and Geospatial Analyst in ArcMap<small>TM</small>. Point data from all of the 2-D resistivity inversions were extracted from RES2DINV<small>TM</small> as x, y, z location data and a resistivity attribute value, and imported into Voxler<small>TM</small>. Data distribution is dense along lines, sparse between lines, and offset vertically by the magnitude of the surface relief (i.e., points are at constant depth below surface, not at constant elevation). In order to generate elevation slices, data were imported into Voxler<small>TM</small> and the resistivity values interpolated vertically using a prolate ellipsoidal search radius with a 2.0 m major axis, a 1.0 m minor axis, and an inverse distance weighting algorithm. The interpolation produced columns of voxles (i.e., a 3-D equivalent of a pixel) with cell dimensions 1.0 m $\times$ 1.0 m $\times$ 0.4 m (x, y, z) and a resistivity value. This interpolation increases the vertical density of data points from five per column to as many as twelve per column. Depth slices at constant elevations were extracted from the Voxler<small>TM</small> model at 0.40 m intervals and imported into ArcMap<small>TM</small>. The data distribution of each at 0.40 m elevation slices was investigated with the aid of semivariograms and histograms in Geostatistical Analyst. To increase the data density to an evenly spaced 2 m grid, data are interpolated between points in the x–y plane. All depth slices were then reintroduced into Voxler<small>TM</small> resulting in a point cloud which provides a 3-D resistivity model.

The relationship between radar facies and resistivity required vertical resistivity profiles to be extracted from the final Voxler<small>TM</small> model along the GPR lines. Resistivity point data and images of the interpreted GPR profiles were also introduced into ArcMap<small>TM</small> and each radar facies digitized into polygons. The polygons were then overlaid onto the resistivity profiles and point values falling within each polygon counted and frequency distribution curves generated and analyzed.

RESULTS AND INTERPRETATION

Trenching

Five trenches were dug for this study: Trench 1 in the abandoned channel and trenches 2–5 on the interior bar platform (Figs. 6, 8; Table 1). Trench 1 (3.3 m deep) consists of three units. Unit 1 (lower) is a 2.0-m-thick, massive, poorly sorted, matrix-supported pebble to cobble gravel with a lower contact below the bottom of the trench. Clasts are
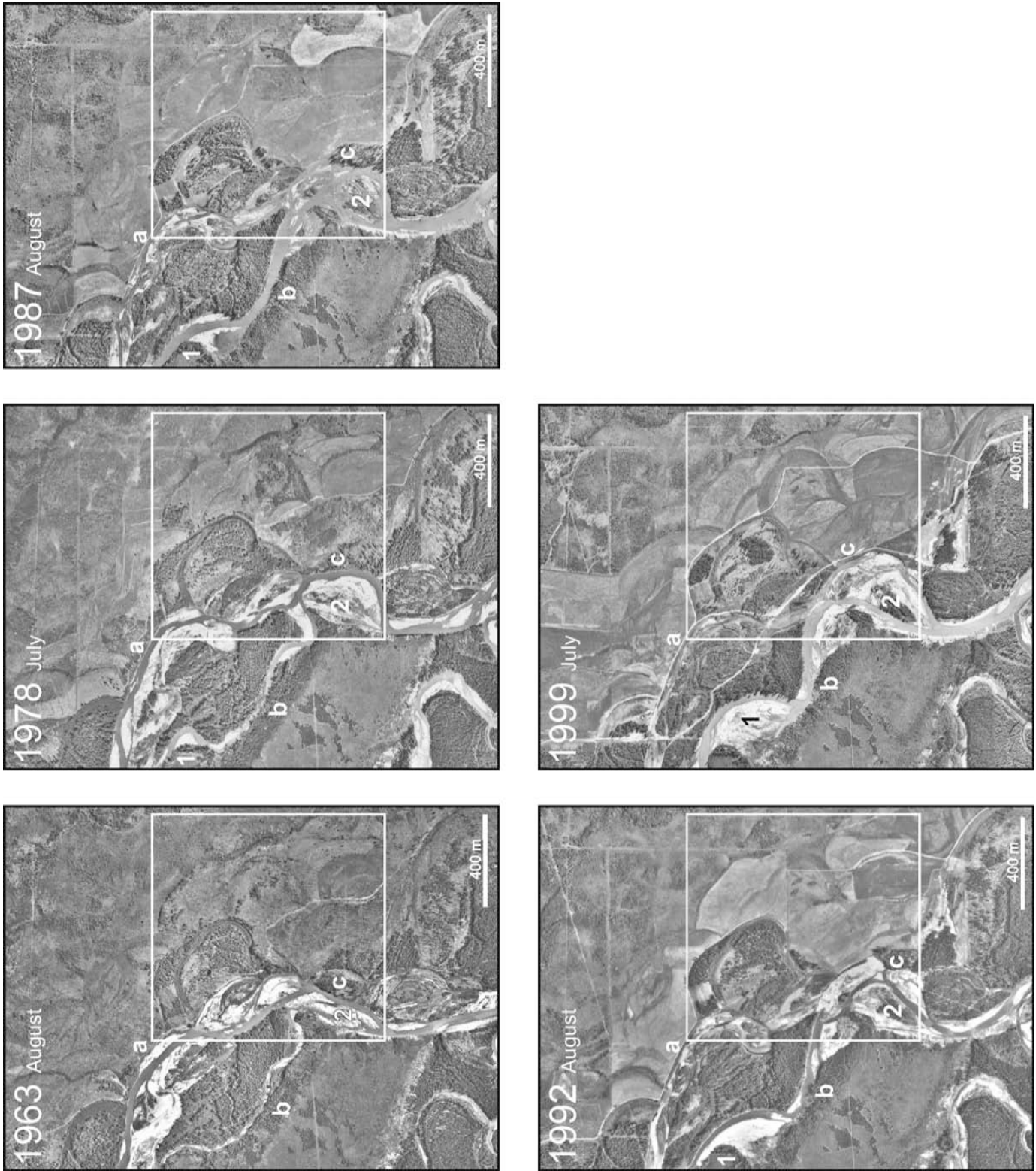
FIG. 4.—Five aerial photographs of Scobie Ranch show the evolution of the floodplain of the Halfway River in the study area (box indicates area in Fig. 6). The numbers refer to bars, and letters to channels. From 1963 to 1987 subordinate *channel b* became the main channel when *channel a* was reduced to a subordinate status and eventually abandoned by 1999. Lateral *bar 1* developed from the eastward migration of *channel b*. *Bar 2* developed from a small lateral bar into a compound bar as *channel c* migrated to the east. *Channel c* eventually became choked with sediment by 1992 and avulsed to a western position by 1999, dissecting *bar 2*. The former positions of *channel c* were subsequently reduced to subordinate status after 1999.

FIG. 5.—*Bar 2* (see Fig. 4) is a likely analog for the development of the features in this study. **A, B)** Migrating gravel sheets preserved on the top of *bar 2*. **C)** Gravel sheet preserved on top of the bar platform in Figure 6. **D)** *Channel c* is an abandoned channel of the Halfway River. **E)** The active channel in 1992 is now vegetated with organic mud overlying gravel. **F)** The organic mud in the former active channel.
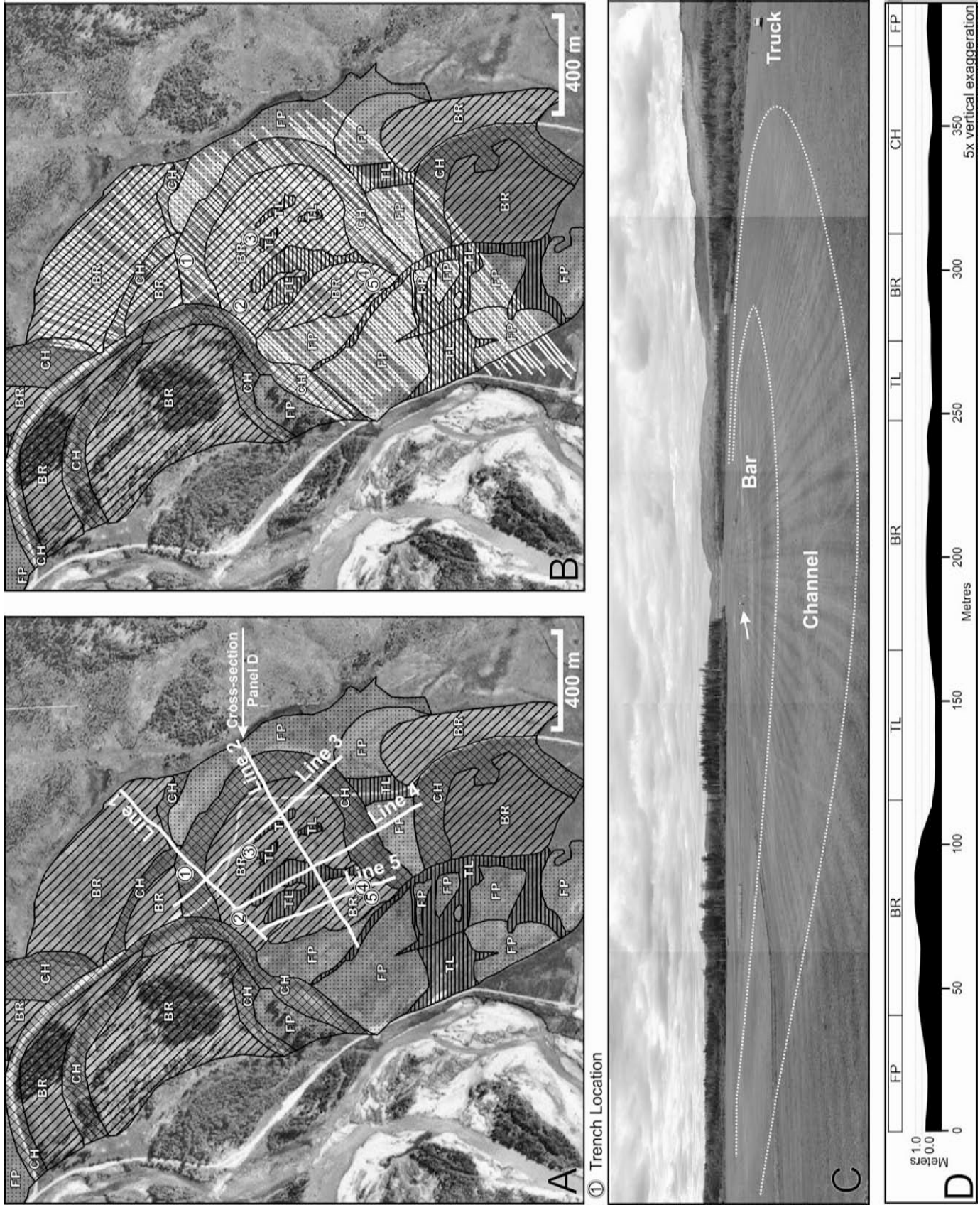
FIG. 6.—The GPR and CCR surveys were conducted over a bar platform and channel bend. The numbers indicate trench locations, and the letters refer to morphostratigraphic units (BR = bar, CH = channel, TL = local topographic low, FP = undifferentiated floodplain). **A)** GPR survey lines (shown in white). **B)** The CCR survey lines (shown in white). **C)** Bar and channel viewed from the southeast end of Line 3 towards the northwest (arrow indicates people for scale). **D)** Topographic profile with morphostratigraphic units along GPR Line 2.
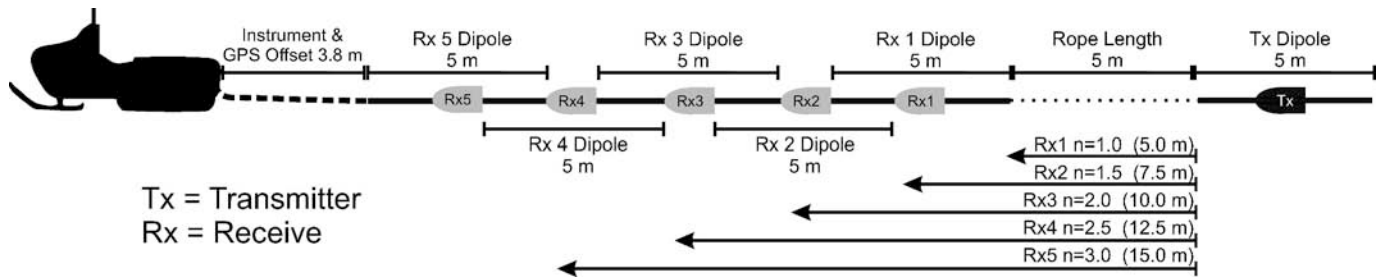
FIG. 7.—OhmMapper configuration with five dipoles and a transmitter (modified from Geometrics 2001).

subangular to well rounded. The matrix is medium sand to coarse granular sand with some silt. Unit 2 (middle) is a 0.6-m-thick, well-sorted, laminated to thin-bedded silty fine sand with dish-shaped lenses of medium sand and both disseminated and layered organic detritus (0.01–0.02 m thick). The lower contact is sharp and undulatory. Unit 3 (upper) is 0.7 m thick and consists of laminated very fine sandy silt with organic detritus. The lower contact is indistinct and gradational over 0.1 m.

Trench 2 (3.6 m deep) is located on the upstream portion of the lower interior bar and consists of three units. Unit 1 (lower) is a 0.5-m-thick clast-supported, massive, poorly sorted, cobble to boulder gravel with a medium to coarse sand matrix and rare pockets of matrix-supported gravel. Many clasts exceed 0.3 m in diameter. A boulder lag occurs at the top of the unit. The lower contact is below the bottom of the pit. Unit 2 (middle) is a 2.85-m-thick, well-stratified, medium-bedded, clast-supported pebble to cobble gravel with minor sand lenses less than 0.1 m thick. Individual beds are horizontal to gently westward-dipping and generally massive. Beds alternate between open-framework, well-sorted, pebble gravel and moderately sorted, pebble to cobble gravel with a medium to coarse sand matrix. Minor westward-dipping planar cross-beds occur. The lower contact is indistinct but marked by a grain size shift, and the boulder lag in the underlying unit. Unit 3 (upper) is 0.25 m thick and consists of laminated, very fine sand and silt with a sharp lower contact.

Trench 3 (3.2 m deep) is located on the interior bar between Trench 2 and the channel, and also reveals three units. Unit 1 (lower) is 0.5 m thick and consists of massive, poorly sorted, matrix- and clast-supported, cobble gravel with rare boulders greater than 0.5 m in diameter. Clasts are slightly more angular than those in the overlying unit. A poorly developed boulder lag occurs at the top of the unit. The lower contact is below the bottom of the pit. Unit 2 (middle) is a 2.2-m-thick, horizontally stratified, thick-interbedded, clast- and matrix-supported, pebble to small cobble gravel. The matrix within the clast-supported beds is coarse sand, whereas the matrix within the matrix-supported beds is medium-grained sand. The lower contact is sharp and marked by the boulder lag. Unit 3 (upper) is a 0.5-m-thick laminated silty, very fine sand with a sharp lower contact.

Trenches 4 and 5 are located on the unit bar west of the interior bar and have consistent stratigraphies also involving three units. Unit 1 (lower) is 0.3 m in Trench 4 and 2.7 m thick in Trench 5 with the lower contact occurring below the bases of the trenches. More of the unit was exposed in Trench 5, where it consists of a coarsening-upwards, crudely stratified cobble gravel. Unit 2 (middle) is 2.2 and 1.3 m thick in trenches 4 and 5, respectively. The unit is a thick-bedded, moderately stratified to massive, clast-supported, large pebble to cobble gravel with a medium-sand matrix. The beds dip gently ($< 10°$) to the south and west in each trench, respectively. The gravel is interbedded with dish-shaped lenses of medium sand, 0.05 to 0.1 m thick, and is laterally continuous for up to 1.0 m. The lower contact is sharp, marked by an increase in clast size with depth. Unit 3 (upper) in both sections is 0.5 m thick and consists of massive and rippled laminated silty, very fine sand with a sharp lower contact.

Ground-Penetrating Radar

The radar profiles typically contain laterally continuous reflections in the upper five meters and abundant diffractions in the lower portions of the profiles (e.g., Figs. 9, 10). Aggressive filtering was applied to enhance the continuous reflection without overly obscuring dipping reflections, though the dipping reflections were affected. Interpretation of the filtered data results in the differentiation of eight radar facies, one radar element (Table 2), and several major bounding reflections. The facies and the element constitute four groups: (1) continuous, horizontal to subhorizonal reflections; (2) clinoform reflections; (3) discontinuous reflections; and (4) concave-up elements. 3-D facies relationships are established where the survey lines cross.

Group 1

Group 1 includes two facies, both of which are represented by continuous, laterally extensive, horizontal, subhorizontal, or slightly inclined ($< 5°$) reflections. Facies 1 has evenly spaced parallel reflections with a uniform frequency between traces. Facies 2 differs from Facies 1 in that individual traces produce reflections of less uniform frequency and tend to be subparallel to slightly hummocky, perhaps the result of constructive/destructive interference or from filtering. These facies dominate the upper 2–3 m of the GPR profiles in the interior bars, secondary channels, but are less common in the main channel.

Interpretation.—These facies are interpreted to be well-stratified horizontally to subhorizontally bedded sediments, suggesting vertical accretion (Wooldridge and Hickin 2005), downstream accretion (Miall 1996), or possibly the horizontal component of cross bedding (Wright 1959).

Group 2

The second group includes the various clinoform reflections. Facies 3 consists of laterally continuous reflections with constant, divergent, or sigmoidal dip patterns. It consistently occurs within the inner bend of the main channel, dipping towards the channel center. Facies 3 also occurs throughout the bar platform with various dip directions. Facies 4 is generally rare, characterized by a shingled pattern, and tends to dip steeper, and is less laterally extensive, than Facies 3. Facies 4 is most notable in Line 2 and 3 at the transition from bar to channel on the inner bank, dipping towards the channel. Facies 5, also rare, has the shortest reflection length and the steepest apparent dip. It occurs on the cutbank side of the channel, dipping towards the channel center, at the base of the channel in Line 4, and in the upper 5 m of Line 5, dipping towards the bar head.

Interpretation.—These facies are interpreted as well-stratified dipping beds. Where facies 3 occurs in the channel, it may represent lateral

migration (Willis 1989; Miall 1996) and channel fill (Bristow 1993); elsewhere it may represent lateral or downstream accretion or bar-margin slip faces (Wooldridge and Hickin 2005). Facies 4 represents lateral accretion. At the cutbank edge, Facies 5 may represent colluvial material while elsewhere it may represent the slip faces of migrating bedforms (Miall 1994).

Group 3

Group three includes discontinuous reflections. These facies form a continuum of reflection patterns, and their classification is relatively arbitrary but focuses on the dominant pattern. Facies 6 is the most coherent of the group and consistently occurs in the base of the main channel. Facies 7 consists of random or chaotic reflections, and Facies 8 consists of diffractions or lenticular reflections. Collectively these discontinuous facies dominate the lower 5 m of all the profiles.

Interpretation.—All of these facies are associated with various concentrations of diffractions in the raw data. Facies 6 and 7 are interpreted as a continuum of crudely stratified to massive deposits. Facies 8 represents a high density of point sources such as cobbles, boulders, or buried logs.

Group 4

Group 4 is represented by Element I. A radar element consists of an association of radar facies in the same way fluvial architectural elements consist of an association of lithofacies (Miall 1996). Element I is defined as a small- to medium-scale feature with a concave-up lower bounding reflection and a variety of internal reflection configurations. This facies is most common in the upper 5 m of the bar platform and within the upper portion of the channel.

Interpretation.—This element is interpreted as filled channels, chutes, or scour-and-fill deposits.

3-D Facies Relationships

At the intersection of GPR lines, a 3-D interpretation of the facies is made (Figs. 11, 12). Because Facies 1 typically occurs adjacent to either another Facies 1 or Facies 2, the orientation of the reflectors is generally horizontal to subhorizontal in 3-D. These are the dominant facies pairing in the upper portion of the profiles across the bar platforms (Fig. 12). There are several exceptions; Facies 1 and 2 occur with dipping reflections in rare cases and therefore represent the horizontal component of cross-bedding (Miall 1996). A poorly developed Facies 2 occurs with a portion of Facies 6, implying that stratification was resolved in only one direction. Other pairings include Facies 3 commonly with Facies 6 and 8, suggesting that crudely stratified dipping beds are resolved in only one direction, and obscured by diffractions in the other. Facies 3 is also paired with Facies 5; reflectors that dip along orthogonal survey lines indicate that each line captured the apparent dip of inclined reflectors. The remaining facies combinations dominate the lower portion of most profiles and include discontinuous reflections in both directions, indicating that these units are crudely stratified, massive, or obscured by diffractions in 3-D.

Bounding Reflections

A boundary is identified in the top 3–5 m of all the profiles, marked by the transition from the more coherent facies (Facies 1–4) to the more discontinuous (Facies 6–8; Figs. 9–12). In some places a strong, laterally continuous (> 100 m) reflection is associated with this facies shift. However, elsewhere the boundary is inferred from the change in reflection geometry. This surface is interpreted as a boundary between two stories: a

deposit of a single channel bar and adjacent channel fill (Bridge and Mackey 1993). The boundary separates deposits interpreted to be moderate to well stratified from crudely stratified, massive, or very coarse deposits. The lower story may represent basal channel sediments, overlain by sheeted bar-platform sediments of the upper story (Mackin 1937; Allen 1963; Walker 1979). Alternatively, the two stories may not be contemporary and therefore represent different generations of floodplains.

Resistivity

The 3-D resistivity model allows a thorough investigation of the distribution of resistivity values. The resistivity values are comparable to those expected for clay, silt, sand, and gravel from ground electromagnetic (EM) survey methods reported by Palacky and Stevens (1990). However, the values are considerably higher than those reported from an airborne EM survey of buried sand and gravel in northeast British Columbia (Best et al. 2006). The resistivity values for fine-grained sediments are comparable to values suggested by Reynolds (1997), but the values he suggests for sand and gravel are much lower than those found in this study. This may be a function of the sediment characteristics or be related to ice in the interstices of the coarse-grained deposit. Based on trench data and surface observations on the morphostratigraphic units, general grain-size prediction can be inferred from the resistivity data. Resistivity values below 400 ohm-m correspond to fine-grained sediments (clay, silt, and fine sand), values between 400 and 800 ohm-m represent medium-grained sediments (sand), and values greater than 800 ohm-m are correlative with coarse-grained sediments (gravel).

Surface resistivity values representing a depth of approximately 0.40 m below the surface correspond well with the morphostratigraphic units mapped from aerial photographs (Fig. 13). Although there are some exceptions, most bar and undifferentiated floodplain features correspond with high resistivity values (> 800 ohm-m) and therefore with coarse sediment. Most depressions and channels, with low resistivity values (< 300 ohm-m), imply sand or fine-grained material. Only the upper portions of major channel features exhibit values less than 100 ohm-m, suggesting fine-grained sediment. In 3-D, the higher resistivity values (> 800 ohm-m) cluster into bodies, connect at the surface, but have an undulating, "basin and dome"-like morphology (Ramsey 1967) at depth surrounded by lower resistivity values at the base of the model.

Two-dimensional resistivity pseudosections were extracted from the 3-D model along the same lines as the GPR survey (Figs. 12, 14). Generally, the profiles show high resistivity values in the upper 2–3 m of areas classified as bar or floodplain morphostratigraphic units, suggesting 2–3 m of coarse sediment, consistent with trench data. The upper 2–3 m in areas classified as topographic lows or channel morphostratigraphic units commonly have low values, suggesting sand or fine-grained channel fill. The lowest resistivity values occur within the main channel scar, again suggesting fine-grained channel fill. However, low values in the channel (though slightly higher than the surface measurements) commonly persist to the base of the profile, suggesting fine-grained sediments at depth, which is inconsistent with the trench data that show gravel in the base of the channel scar (Fig. 8). This discrepancy is in part related to skin-depth effect, but more importantly the conductive surface material (fine-grained sediment) provides a preferential path for current to flow, essentially blocking current from flowing into deeper units (Geometrics 2001). Resistivity values for sediments deeper than 2 m below the fine-grained channel fill are, consequently, suspect.

There are exceptions to these generalizations. For example, in Line 3 there is no significant change in the high resistivity values in the upper 2 m from the bar across the poorly developed topographic low and back to the bar. In Line 4, high resistivity values characterize the northwest portion of the topographic low, although resistivity decreases to the
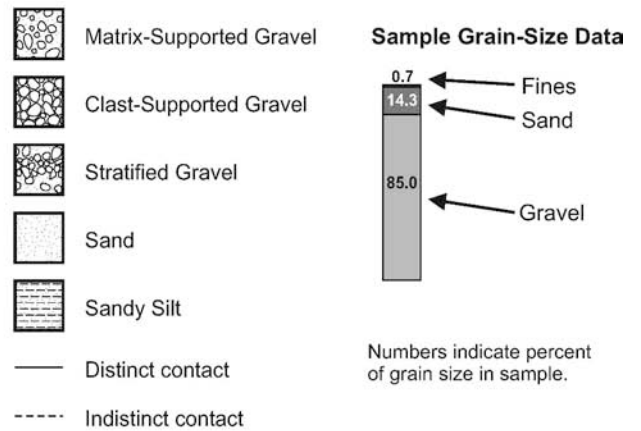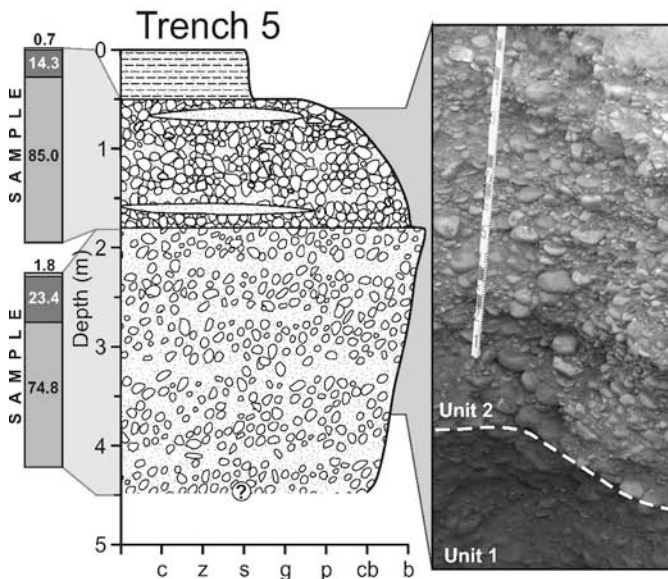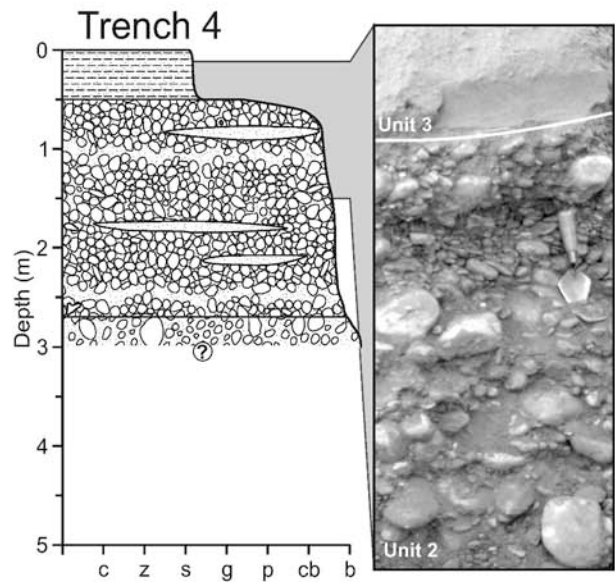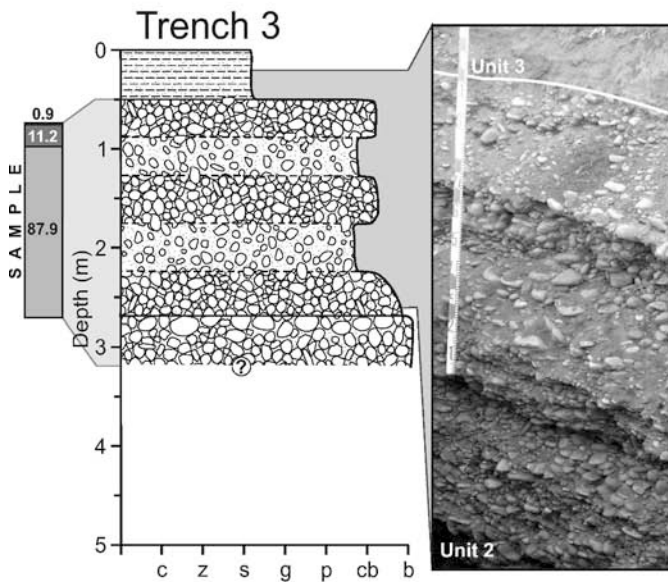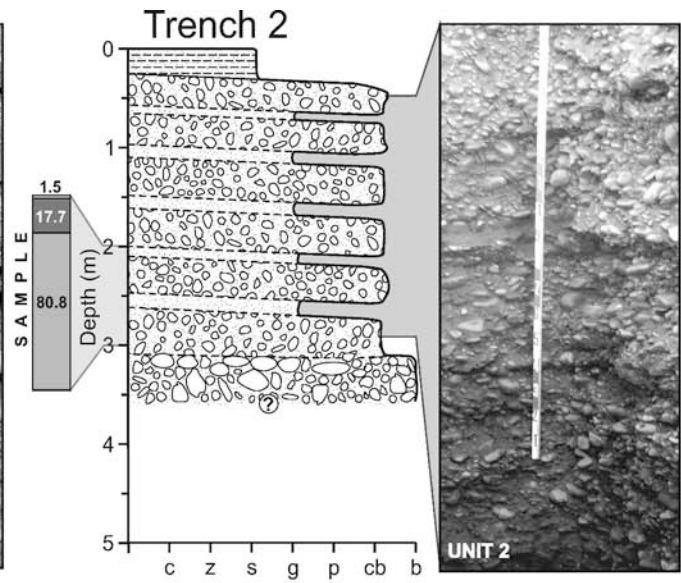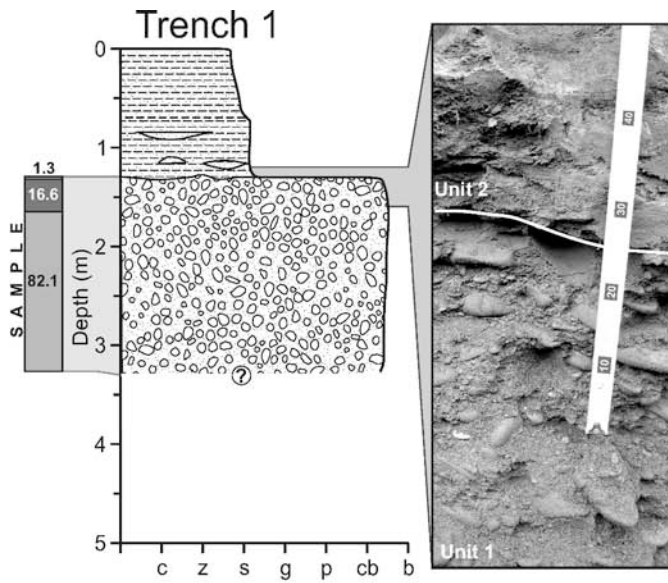
TABLE 1.—*Summary of trench data.*

Testpit	Depth (m)	Lithofacies (Modified from Miall 1996)
1	0–0.7	Fl
	0.7–1.3	Fl, Sm
	1.3–3.3	Gmm
2	0–0.25	Fl
	0.25–3.1	Gcm, Gcp, Sm
	3.1–3.6	Gcm, Gmm
3	0–0.5	Fl
	0.5–2.7	Gcp, Gmp
	2.7–3.2	Gmm
4	0–0.5	Fl, Sr
	0.5–2.7	Gcm, Sm, Gcg
	2.7–3	Gmm, Gmi
5	0–0.5	Fl
	0.5–1.8	Gcm, Gcp, Sm
	1.8–4.5	Gmm, Gmi

Fl: Fines; laminated.
Gcm: Gravel; clast supported; massive.
Gcp: Gravel; clast supported; planar stratified.
Sm: Sand; massive
Gcg: Gravel; clast supported; graded.
Sr: Sand; rippled
Gmm: Gravel; matrix supported; massive.
Gmp: Gravel; matrix supported; planar stratified.
Gmi: Gravel; matrix supported; inverse grading.

southeast as this topographic low passes into a more developed channel. This suggests that the low values are more likely to occur where depressions and channel features are better developed.

Combined GPR and Resistivity

The GPR and CCR surveys are directly combined to explore the relationship between the radar facies and distribution and magnitude of resistivity values within each facies. The shape of the distributions can indicate sorting, and the magnitude of the resistivity values is used as a proxy for grain size (Fig. 14). Narrow distributions with consistent resistivity values are taken to represent well-sorted material, and wide distributions represent more poorly sorted material. Overall there is reasonable visual correlation between facies and resistivity, with sharp changes in resistivity roughly coinciding with facies boundaries (Fig. 14). This was encouraging, insomuch as the facies boundaries are determined independently of the resistivity data.

The distribution of resistivity values within individual facies polygons are classified into seven general shapes (Fig. 15): (a) log-normal low variability; (b) log-normal moderate variability; (c) log-normal highly variable; (d) log-skewed left; (e) log-skewed right; (f) log-bimodal; and (g) log-multimodal.

Shapes *a*, *b*, and *c* all have log-normal distributions but have progressively larger standard deviations. This is interpreted as indicating good sorting in *a*, moderate sorting in *b*, and poor sorting in *c*. Shapes *d* and *e* have positively and negatively skewed patterns, respectively. Shape *d* has a relatively narrow region of dominant resistivity values flanked by subordinate lower values whereas shape *e* is flanked by subordinate higher values. These distributions represent a dominant grain size with subordinate finer-grained or coarser-grained material, respectively.

Alternatively, these shapes may result from the poor fit of the GPR facies to the resistivity data, erroneously incorporating values from adjacent units. Shapes *f* and *g* include distributions with two or more distinctive peaks. Bimodal Shape *f* represents two dominant grain-sizes and can have a wide range or a relatively narrow range of resistivity values. Multimodal Shape *g* generally spans a wide range of resistivity values, indicating poor sorting.

The dominant grain size for each polygon uses the surface grain-size classes noted earlier (i.e. < 400 ohm-m = fine-grained; 400–800 ohm-m = sand; > 800 ohm-m = gravel). Grain size for each polygon is assigned by noting where the largest area under the log-transformed frequency curve falls on the resistivity spectrum (e.g., Fig. 14). If a distribution spans more than one class, the polygon is considered to be composed of a mix of sediment. A summary of the grain size, sorting, and associated radar architecture is presented in Table 3.

A resistivity drop consistently occurs across the major bounding reflection (story boundary) noted in the GPR survey. This sharp resistivity drop is coincident with the transition between the horizontal to subhorizontal radar facies (Group 1) and the more discontinuous facies below. As previously noted, this story boundary occurs between well-stratified upper gravel and the poorly sorted lower gravel observed in the trenches.

DISCUSSION

The Case Study

The objective of this study is to develop a methodology of combining sedimentology, GPR, and CCR for geophysical architecture analysis in fluvial environments. The trenches provide direct observation of the preserved lithofacies in the morphostratigraphic units and stratigraphies for the channel and bar platform on which to base the interpretation of the radar and resistivity data. The trench data are summarized in two idealized vertical sections (Fig. 16): one represents the channel fill, the other the interior bar platform. The lower gravel portion of channel-fill succession represents bedload transported in an active channel (e.g., Fig. 5D). This is overlain by laminated silty fine sand deposited mainly from suspension during waning flow or from periodic flooding of the abandoned channel. The upper laminated organic-rich fine sand and silt represents deposition in standing water following channel abandonment. This stratigraphy is consistent with the unstable or abandoned channels of wandering gravel-bed rivers, described by Desloges and Church (1987) and Brierley and Hickin (1992)

The lower portion of the interior bar consists of poorly sorted cobble to boulder gravel capped by a boulder lag. This unit is interpreted as a high-energy gravel deposit that was subsequently winnowed. This unit is overlain by horizontal to gently inclined, well-stratified pebble to cobble gravel interpreted to be stacked gravel-bedload sheets (Fig. 5B) (Whiting et al. 1988; Ashmore 1991). The upper unit consists of laminated sandy silt deposited mainly from suspension as overbank sediments. This fining-upward sequence is consistent with bar and floodplain stratigraphy of a wandering gravel-bed river (Allen 1983; Desloges and Church 1987; Brierley 1991; Nanson and Knighton 1996; Passmore and Macklin 2000).

The processed GPR data reveal two domains: the upper portion, dominated by Groups 1, 2, and 4 radar facies, and the lower, dominated by Group 3 facies. In the upper domain, Groups 1 and 4 are common across the bar core, indicating that the bar platform is dominated by well-stratified, horizontal to subhorizontal sediments occasionally dissected by

←

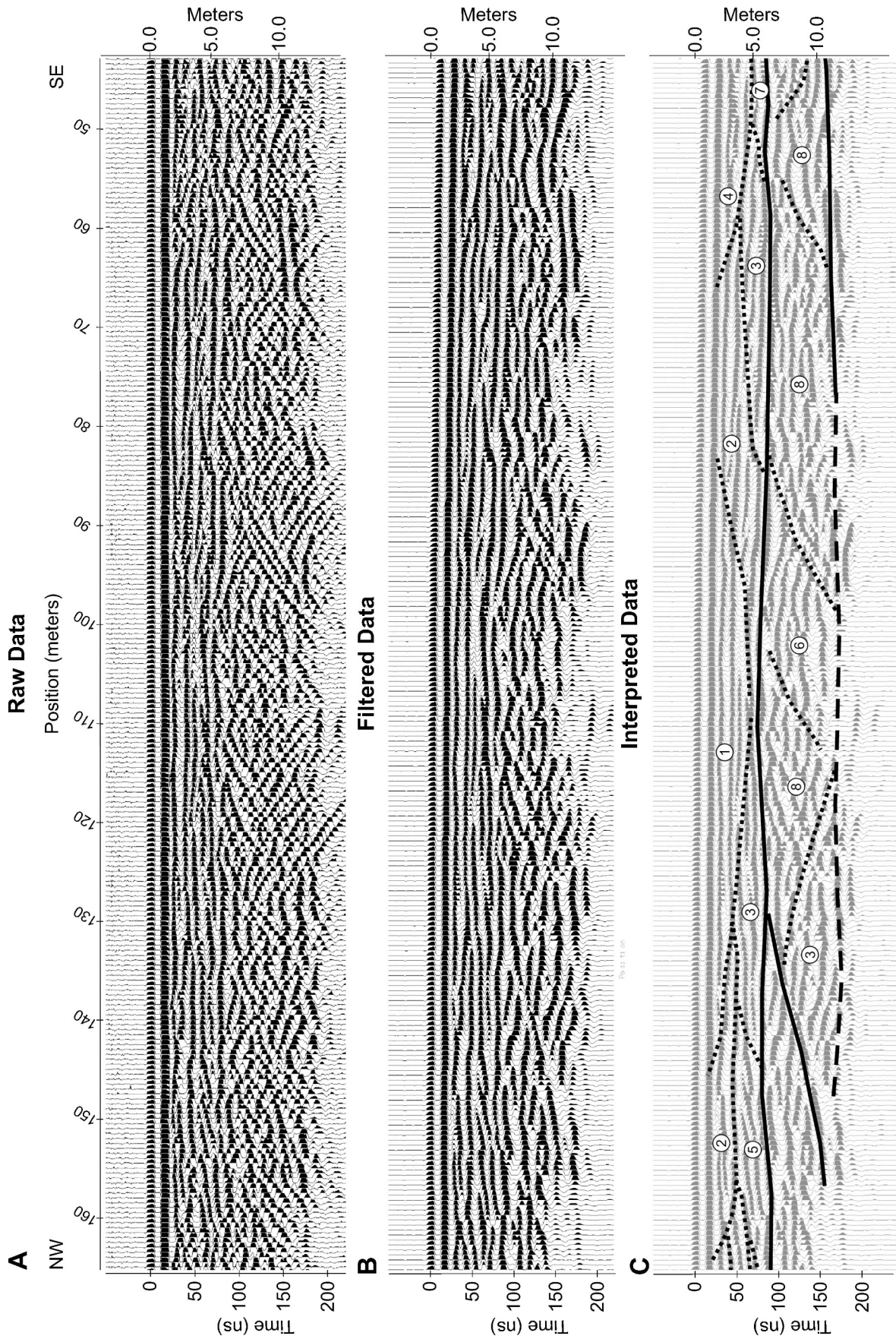FIG. 8.—Trench stratigraphy of the bar platform and channel (locations in Fig. 6).

FIG. 9.— A portion of GPR Line 5 located across the bar platform. **A)** Raw data; **B)** filtered data; **C)** interpreted data (see Table 2).
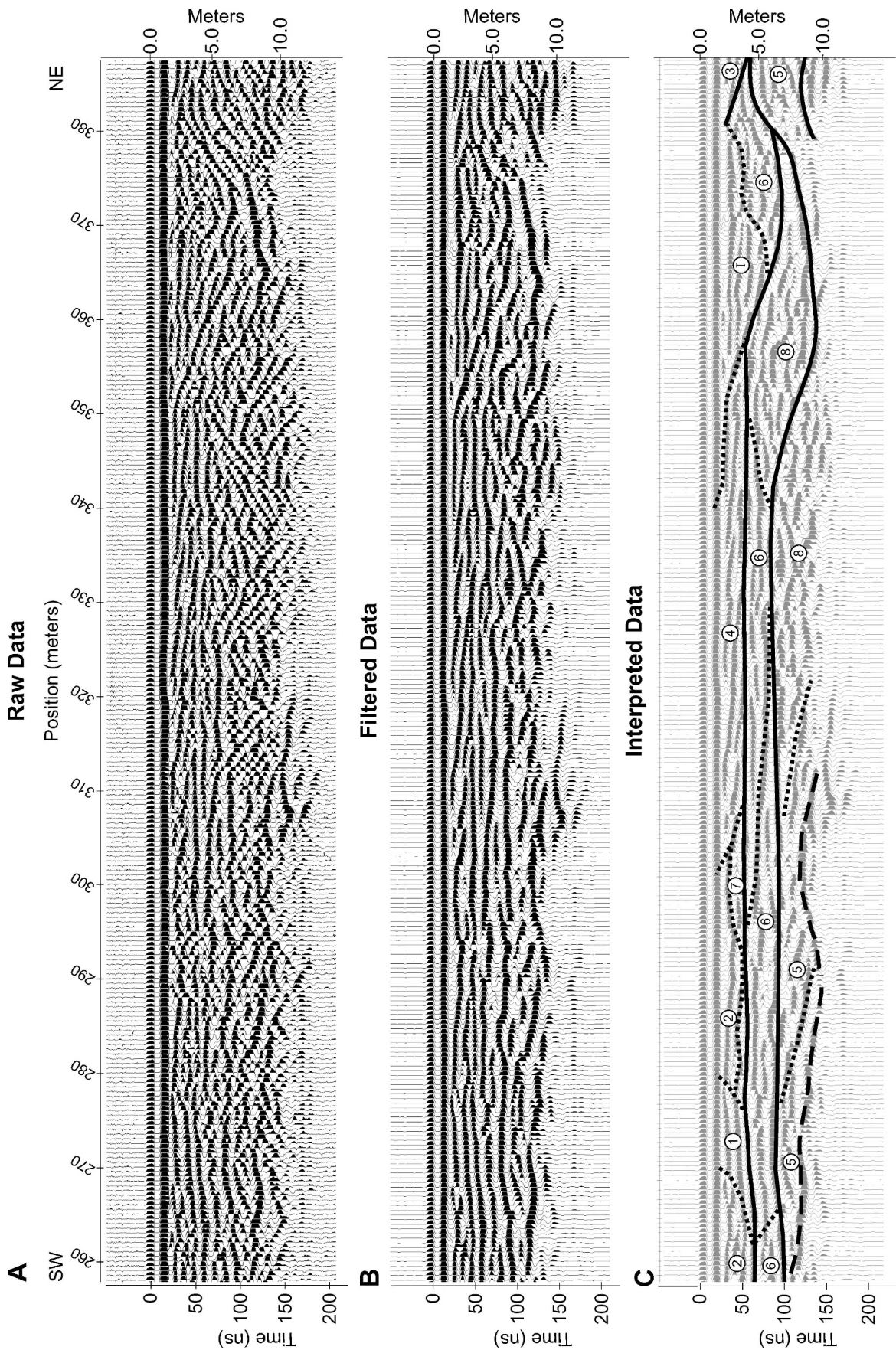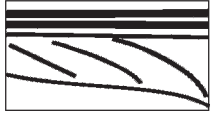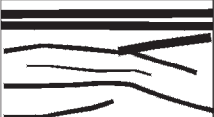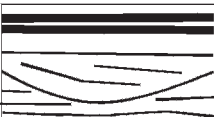
FIG. 10.—A portion of GPR Line 2 located at the transition from the bar platform to the channel. **A)** raw data; **B)** filtered data; **C)** interpreted data (see Table 2).

TABLE 2.—*Four groups of radar facies and their interpretation.*

Group	Category	Description	Interpretation	Schematic Example
1	Continuous Horizontal to Subhorizontal	Facies 1 — Laterally continuous (10–70 m), parallel, even, uniform, horizontal to subhorizontal reflections.	Well stratified, horizontal bedding. Vertical accretion, horizontal component of cross-bedding.	
		Facies 2 — Laterally continuous (10–70 m), non-uniform, subhorizontal (0–<10°) to weakly hummocky, parallel to subparallel reflections.	Moderately stratified subhorizontal to slightly inclined bedding. Vertical accretion, downstream accretion, horizontal component of cross-bedding.	
2	Clinoform	Facies 3 — Laterally continuous (15–60 m), low-angle (1–20°), sigmoidal to divergent reflections.	Well to moderately stratified, dipping bedding. Lateral or downstream accretion, migrating bar or bedform, prograding channel fill.	
		Facies 4 — Moderately continuous (5–30 m), inclined (5–20°), shingled reflections.	Well to moderately stratified dipping bedding. Lateral accretion, slipface of migrating bedform.	
		Facies 5 — Short (5–10 m), oblique, tangential or parallel, inclined (15°–30°) reflections.	Moderately to poorly stratified dipping bedding. Lateral accretion, slipface of migrating, cutbank colluvium.	
3	Discontinuous	Facies 6 — Discontinuous (5–15 m), hummocky or disrupted reflections.	Crudely stratified to massive deposit obscured by diffractions	
		Facies 7 — Discontinuous (5–10 m), random, chaotic reflections.	Crudely stratified to massive deposit obscured by diffractions	
		Facies 8 — Discontinuous, abundant diffracted reflections	Abundant point source diffraction from objects such as large cobbles, boulders, or logs.	
4	Concave-up Lower Boundary	Element I — Small- to medium-scale (10–30 m), concave-up lower bounding surface, internal reflection geometry includes onlap, mounded onlap, divergent, prograding, chaotic, or complex fills.	Sediment-filled chute or channel	

Facies: 1-1; 1-2; 2-2   Facies: 1-Element I;   Facies: 1-3; 2-3; 1-4; 2-4
                              2-Element I   1-5; 2-5

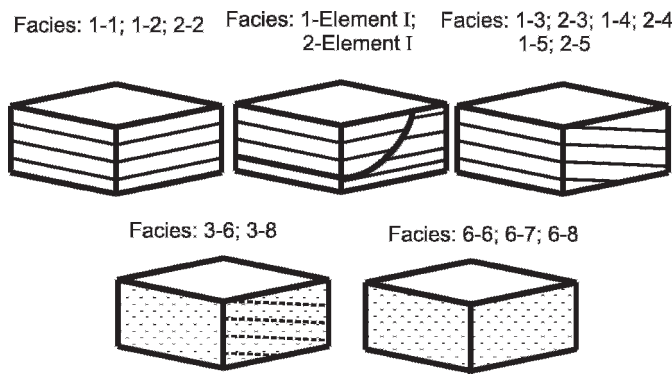Facies: 3-6; 3-8   Facies: 6-6; 6-7; 6-8

FIG. 11.— Radar facies pairings and 3-D reflection orientations from the intersection of GPR lines.

channels (Element I). Resistivity values for facies in the bar core are typically high, and have relatively narrow distributions, suggesting that gravel is the dominant grain size (consistent with trench data). Therefore, the prevailing depositional process across the bar platform was vertical accretion of gravel sheets. Sheeted deposits are well documented in modern and ancient braided and wandering rivers (Smith 1974; Ferguson and Werritty 1983; Desloges and Church 1987; Roberts et al. 1997; Wooldridge and Hickin 2005; Passmore and Macklin 2007).

The main topographic low that dissects the bar platform has architecture similar to that of the adjacent bar core, but resistivity values are lower and more varied where it forms a distinct channel (intersection of Lines 2 and 4). The resistivity predicts finer-grained sediment in this area despite a GPR signature consistent with the rest of the bar. This portion of the topographic low is therefore interpreted as a different architectural element, a subordinate channel with subhorizontally stratified sand or a mix of fines, sand, and gravel fill.

The transition from bar to channel in the upper portion of Lines 2 and 3 shows that the dominant depositional process was lateral accretion of moderately to poorly sorted or mixed sand and gravel (Facies 4). This suggests that the bar platform transitions from vertical accretion in the core to lateral and downstream migration on the mid to downstream section of the outer-platform margin. The radar facies within the main channel show consistency. Facies 6 or 8 typically occur in the base of the channel, indicating massive deposits or coarse sediment (abundant point sources), such as cobbles and boulders. Unfortunately, the base of the channel is below the maximum depth of reliable CCR data, so it is speculated that these facies represent basal-channel gravel. Where Facies 3 occurs in the upper 2–3 m on the inner bank of the channel, dipping towards the channel center, resistivity values are indicative of sand. Here, Facies 3 represents channel fill dominated by lateral progradation from the bar platform into the main channel. The remainder of the channel consists of fine-grained subhorizontal (Facies 2) channel fill and Element I, small channels, chutes, or scours with fine-grained sediment fill. The GPR signature alone is insufficient to differentiate Facies 2 in the bar core from Facies 2 in the channel fill, but the inclusion of resistivity data enables these facies to be separated into different architectural elements.

Geomorphology alone might lead this morphostratigraphic assemblage to be classified as a laterally migrating channel bend consistent with the classic meander model. The GPR-CCR surveys reveal instead that this channel bend essentially is an avulsion feature, and a four-phase model is invoked to explain the radar facies and resistivity model (Fig. 17). The bulk of gravel transport and deposition occurs during flood. Sheets of gravel are transported as bedload along the bar surface during peak discharge (Phase I). As stream power declines and flow wanes, the gravel sheets essentially freeze in place and suspended sediment is deposited over the sheeted gravel. As water levels drop, the gravel bodies emerge as an interior bar (Phase II). The main channel becomes established as a river bend, and the sheeted gravel becomes the core of the bar platform. Clinoforms common on the mid to downstream margin of the bar platform (Facies 4) suggest that once the main channel became established, lateral migration and reworking of the existing floodplain commenced (Phase III). The final phase is marked by avulsion and abandonment of the channel (Phase IV). During this phase, periodic flooding or water stagnation results in the slow accumulation of organic mud. The discrepancy between planform and expected architecture reinforces an important caution: landform genesis can be established reliably only if the 3-D internal structure and composition are known.

Methodology

When combined, outcrop data (trenching), GPR, and CCR are effective subsurface investigative tools. Outcrop data provide sedimentological and stratigraphic context, which in turn is used to calibrate the geophysical data. Indirect geophysical methods require, or at least benefit from, calibration from direct observation because most geophysical techniques produce non-unique solutions. Hence modeling and interpretation may be subjective. Geophysical interpretations are more reliable when developed from observation. Geophysics does, however, extend investigation beyond exposed outcrop and can be an efficient and powerful tool for subsurface investigation.

The OhmMapper™ instrument is a practical resistivity tool, and the data effective for estimating the grain size in the upper 5 m of the floodplain. The data collection is relatively simple and efficient. The inverted data produce geologically plausible pseudosections that are generally compatible with surface and trench observations. The procedure for incorporating the 2-D resistivity pseudosection into a coherent 3-D subsurface model combines geophysical inversion software with established geospatial techniques and offers a relatively cost-effective method of generating a versatile 3-D resistivity model. The GIS platforms and tools used are neither specialized nor proprietary geophysical modeling software, but instead are common, commercial GIS products.

The approach presented in this study is relatively novel and is considered a foundation on which to build. Improvements will undoubtedly benefit future studies. For example, the GPR data are aggressively filtered to enhance reflections obscured by diffractions. More sophisticated processing, such as migration, is more effective at revealing coherent dipping reflections or those obscured by diffractions. Additional processing may therefore clarify some GPR data (Neal 2004). Multi-frequency GPR may also enhance the interpretation of radar facies. Because the resolution of GPR is dictated by the central operating frequency of the survey, interpretation of radar facies as fluvial lithofacies or architectural elements benefits from multi-frequency surveys along each line (Wooldridge and Hickin 2005; Mumpy et al. 2007). The correlation between resistivity values and grain size are essentially empirical in this study. Direct, *in situ* measurement of the resistivity values with respect to lithofacies would quantify the resistivity results, thereby improving the prediction of grain size from resistivity data. These data can be incorporated directly into the inversion parameters, refining the model. Addressing conductive surface sediment, such as in the main channel, will improve the model. Resistivity values below the fine-grained channel fill were not indicative of gravel in the channel bottom as was observed in the trenches. This inconsistency may be addressed by adjustment and fine-tuning of the inversion parameters or by changing instrument configuration to extend the depth of the pseudosection (e.g., using 10 m dipoles). Addressing conductive surface sediments will be particularly important in future surveys where thick, fine-grained deposits
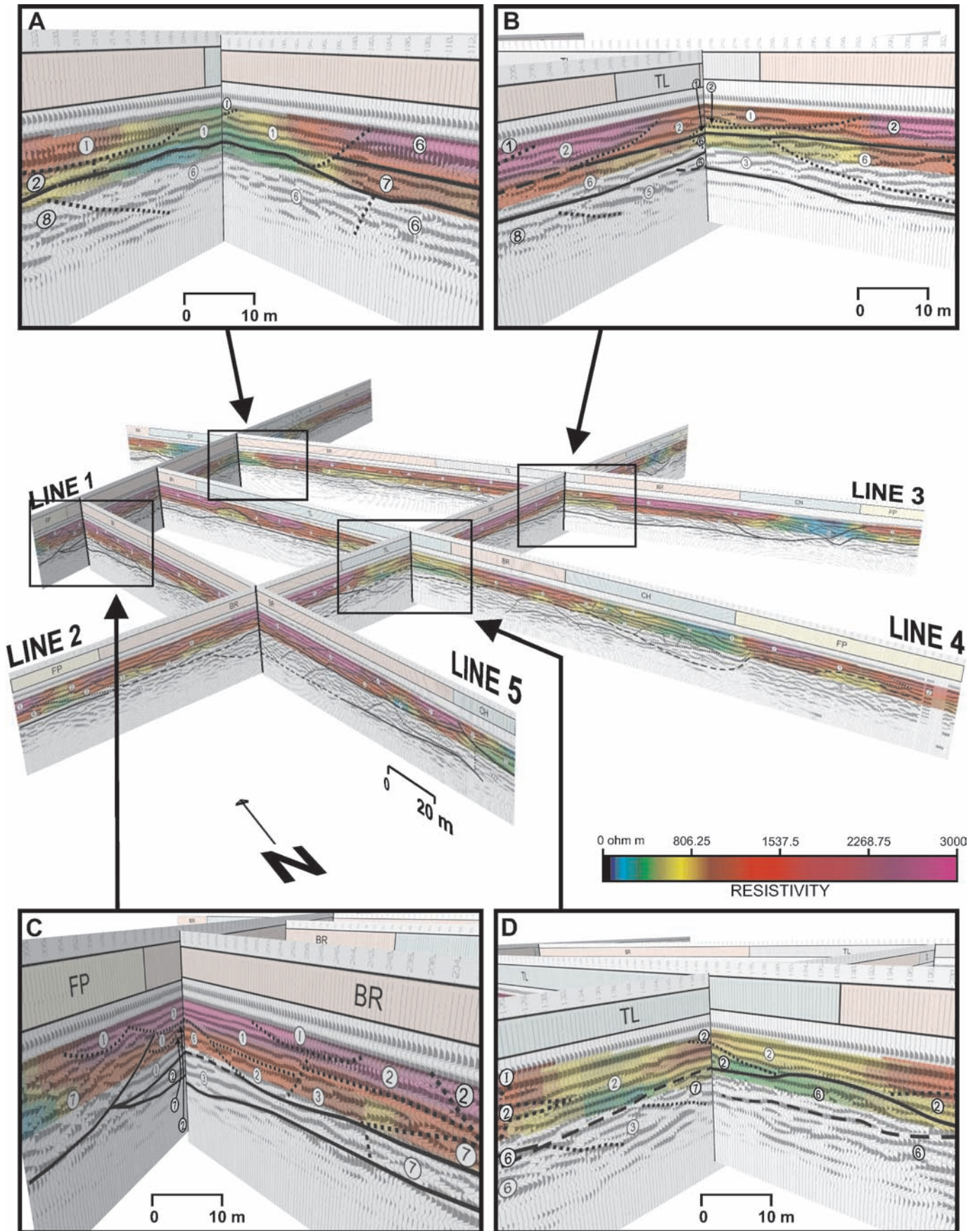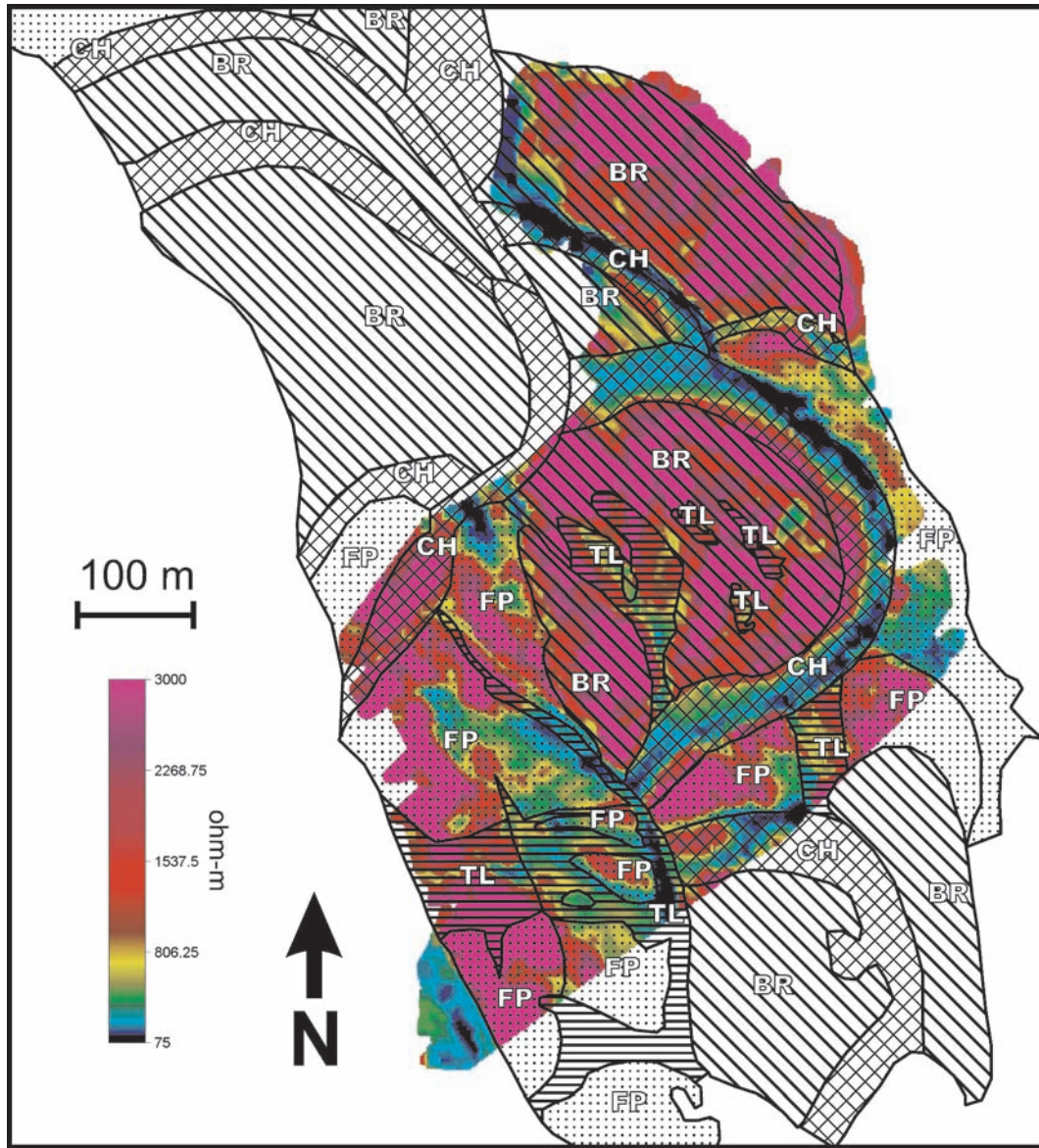
Fɪɢ. 13.—The surface resistivity correlates well with the morphostratigraphic units derived from the aerial photographs (BR = bar, CH = channel, TL = local topographic low, FP = undifferentiated floodplain).

are substantial fluvial-architecture elements (e.g., overbank environments). In terms of direct comparison of GPR and CCR data, the scale and resolution of the two geophysical techniques used in this study are not entirely compatible. The radar facies established with the 100 MHz antenna resolved mesoscale features, whereas the resolution of the resistivity data is more comparable to the mesoscale to macroscale features (Miall 1996). Some error was introduced because of this discrepancy in scale. Integrating the GPR facies boundaries and bounding surfaces directly into the inversions parameters would enhance the fit of two data sets.

Despite these considerations, this study confirms the utility of combining GPR and CCR for indirect fluvial architectural analysis. Because this study was conducted on a poorly developed wandering gravel-bed river, the logical next step is to apply the methodology to morphostratigraphic units in end-member river planforms preferably with historic records in order to establish a link between fluvial style and preserved subsurface elements. The method will also benefit studies relating subsurface features that produce GPR reflections and host material (volumes) with contrasting electrical properties (e.g., subsurface contamination, buried cavities, and coal and stratiform-mineral exploration).

←

Fɪɢ. 12.—Resistivity data from the 3-D model overlaid onto the GPR lines. The numbers refer to radar facies from Table 2, the dashed lines are facies boundaries, and the solid lines are storey boundaries. **A)** Upstream margin of bar platform and channel. **B)** Small subtle topographic low on bar platform. **C)** Upstream margin of bar platform. **D)** Well developed topographic low within bar platform.
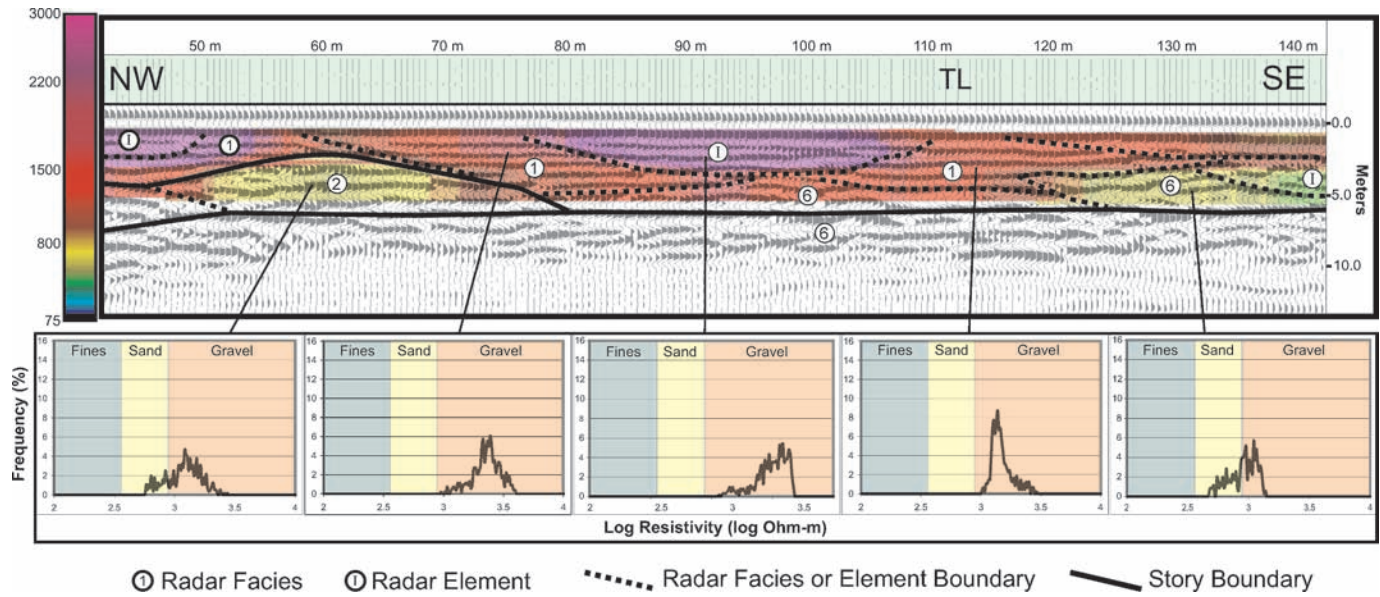
FIG. 14.—Example of combined GPR and CCR from a portion of GPR Line 4 with resistivity distributions and corresponding grain size for several GPR facies.

CONCLUSIONS

This study directly combines GPR and CCR to image fluvial architecture and grain-size distribution of a bar platform and channel on the floodplain of a poorly organized wandering gravel-bed river.
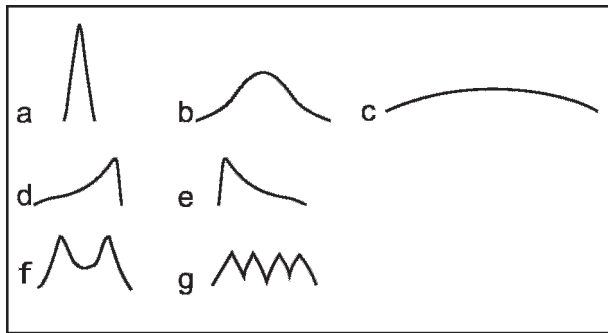

FIG. 15.— Simplified Resistivity-value distribution shapes used as a proxy for grain size and sorting for each radar facies polygons (Table 3).

Although GPR is routinely used to image fluvial architecture, most GPR studies do not include grain size in the radar-facies evaluation. This information is critical to fluvial architectural analysis, insomuch as architecture and grain size are integral to the classification terminology proposed by Miall (1996). This study demonstrates that CCR adds a grain-size proxy to traditional GPR studies essential for geophysical fluvial architectural analysis. The methodology presented uses field observations to calibrate the geophysical data. Trenches provide lithofacies and stratigraphy from which geophysical interpretation and inversion parameters are based. The reflectors imaged in a 100 MHz GPR survey are taken to represent bed orientation and major bounding surfaces. The resulting radar facies are interpreted as mesoscale and small macroscale fluvial-architecture units. The inverted and modeled CCR data are used as a proxy for grain size, where high values correspond with coarse sediment and lower values with fine-grained material. The direct comparison of resistivity values with the GPR facies reveals that GPR architecture is not independent of grain size and that GPR facies may be common to both a coarse-grained and a fine-grained unit, in which case they represent separate fluvial architectural elements. The combination of
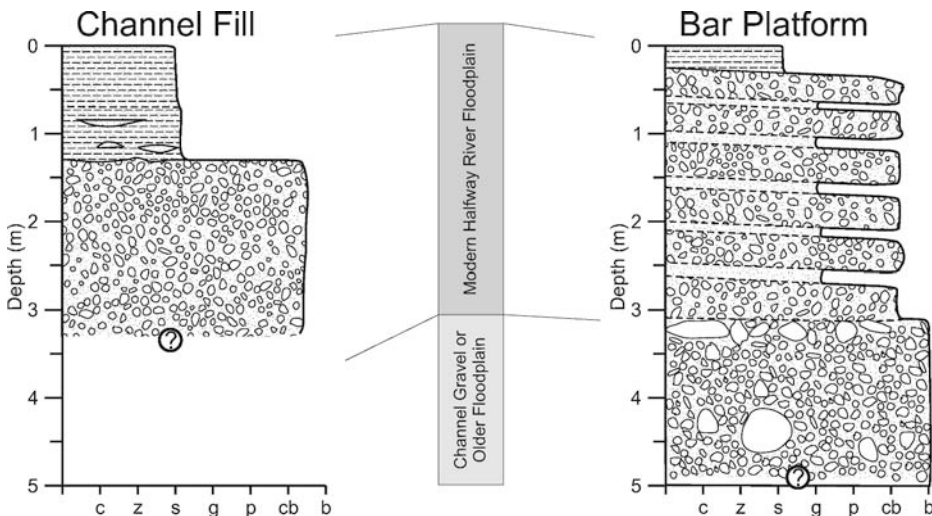

FIG. 16.—Two idealized vertical sections representing the stratigraphy of the channel fill and the bar platform from trench data.

TABLE 3.—*Combined radar facies and the distribution of resistivity values were interpreted in terms of grain size, sorting, and achitecture.*

| Radar Facies	Grain-size and Sorting from Resistivity Distribution	Architectural and grain-size Interpretation	No. Occurrences by Radar Facies
1	Moderately sorted coarse-grained unit	Horizontally stratified gravel	8
1	Moderate to well sorted coarse-grained unit	Horizontally stratified gravel	3
1	Well sorted medium-grained unit	Horizontally stratified sand	3
1	Two distinct coarse-grained units	Horizontally stratified gravel	2
1	Moderately sorted coarse-grained unit	Horizontally stratified sand and gravel	1
1	Poorly sorted fine- to coarse-grained unit	Horizontally stratified fines, sand, and gravel	1
1	Two distinct medium- to coarse-grained units	Horizontally stratified sand and gravel	1
1	Well sorted coarse-grained unit	Horizontally stratified gravel	1
1	Well sorted medium- to coarse-grained unit	Horizontally stratified sand and gravel	1
2	Poorly sorted medium- to coarse-grained unit	Subhorizontally stratified sand and gravel	10
2	Well sorted coarse-grained unit	Subhorizontally stratified gravel	8
2	Moderately sorted coarse-grained unit	Subhorizontally stratified gravel	7
2	Poorly sorted coarse-grained unit	Subhorizontally stratified gravel	4
2	Poorly sorted fine- to coarse-grained unit	Suborizontally stratified fines, sand, and gravel	3
2	Moderate to well sorted medium-grained unit	Subhorizontally stratified sand	2
2	Moderate to well sorted medium- to coarse-grained unit	Subhorizontally stratified sand and gravel	1
2	Moderately sorted fine- to medium-grained unit	Subhorizontally stratified fines and sand	1
2	Moderately sorted fine-grained unit	Subhorizontally stratified fines	1
2	Moderately sorted medium- to coarse-grained unit	Subhorizontally stratified sand and gravel	1
2	Moderately sorted medum-grained unit	Subhorizontally stratified sand	1
2	Poorly sorted fine- to medium-grained unit	Subhorizontally stratified fines and sand	1
2	Two distinct coarse-grained unit	Subhorizontally stratified gravel	1
2	Two distinct coarse-grained units	Subhorizontally stratified gravel	1
2	Two distinct fine-grained unit	Subhorizontally stratified fines	1
2	Two distinct medium-grained units	Subhorizontally stratified sand	1
2	Well sorted medium-grained unit	Subhorizontally stratified sand	1
3	Poorly sorted fine- to coarse-grained unit	Dipping stratified fines, sand, and gravel	5
3	Moderately sorted coarse-grained unit	Dipping stratified gravel	3
3	Poorly sorted medium- to coarse-grained unit	Dipping stratified sand and gravel	2
3	Moderately sorted fine- to medium-grained unit	Dipping stratified silty fine sand	1
3	Poorly sorted fine- to medium-grained unit	Dipping stratified fines and sand	1
4	Moderately sorted coarse-grained unit	Dipping stratified gravel	1
4	Moderately sorted medium- to coarse-grained unit	Dipping stratified sand and gravel	1
4	Two distinct coarse-grained unit	Dipping stratified gravel	1
5	Poorly sorted coarse-grained unit	Dipping moderately stratified gravel	1
5	Poorly sorted fine- to medium-grained unit	Dipping crudely stratified fines and sand	1
5	Well sorted medium-grained unit	Dipping crudely startified sand	1
6	Poorly sorted medium- to coarse-grained unit	Massive to crudely stratified sand and gravel	9
6	Poorly sorted coarse-grained unit	Massive to crudely stratified gravel	2
6	Poorly sorted fine- to coarse-grained unit	Massive to crudely stratified fines, sand, and gravel	2
6	Moderately sorted coarse-grained unit	Massive to crudely stratified gravel	1
6	Moderately sorted fine- to medium-grained unit	Massive to crudely stratified fines	1
6	Moderately sorted fine- to medium-grained unit	Massive to crudely stratified fines and sand	1
6	Two distinct coarse-grained unit	Massive to crudely stratified gravel	1
6	Well sorted coarse-grained unit	Massive to crudely stratified gravel	1
6	Well sorted fine- to medium-grained unit	Massive to crudely stratified fines and sand	1
7	Poorly sorted medium- to coarse-grained unit	Massive sand and gravel	4
7	Poorly sorted fine- to coarse-grained unit	Massive fines, sand, and gravel	2
7	Moderately sorted medium-grained unit	Massive sand	1
7	Poorly sorted coarse-grained unit	Massive gravel	1
7	Well sorted medium- to coarse-grained unit	Massive sandy gravel	1
8	Moderately sorted coarse-grained unit	Massive gravel (boulders?)	1
8	Poorly sorted fine- to coarse-grained unit	Massive sand and gravel (boulders?)	1
8	Well sorted medium-coarse grained unit	Massive sand and gravel (boulders?)	1
Element I	Well sorted coarse-grained unit	Gravel channel fill	7
Element I	Moderately to well sorted coarse-grained unit	Gravel channel fill	6
Element I	Moderately sorted coarse-grained unit	Gravel channel fill	4
Element I	Poorly sorted fine- to coarse-grained unit	Fines, sand, and gravel channel fill	4
Element I	Moderately sorted medium- to coarse-grained unit	Sand and gravel channel fill	2
Element I	Poorly sorted fine- to medium-grained unit	Fines and sand channel fill	2
Element I	Poorly sorted medium- to coarse-grained unit	Sand and gravel channel fill	2
Element I	Moderately sorted medium-grained unit	Sand channel fill	1
Element I	Poorly sorted coarse-grained unit	Gravel channel fill	1
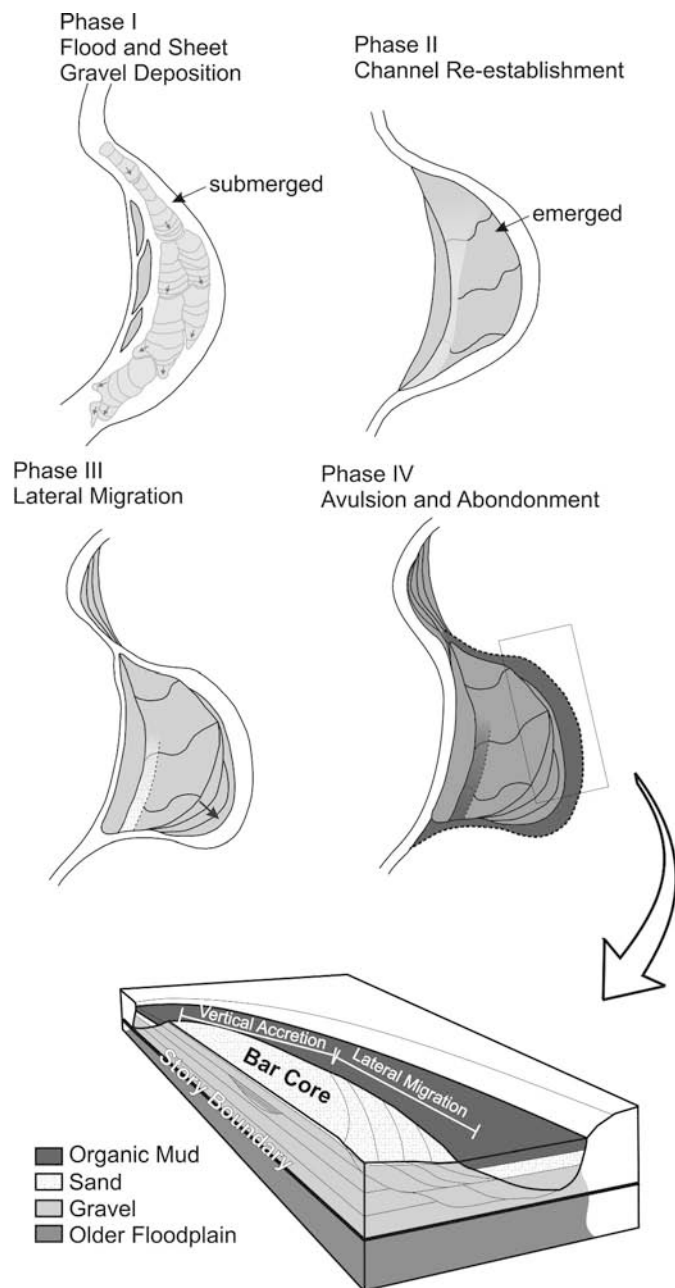
FIG. 17.— The evolution of the bar and channel based on the combined sedimentology, GPR, and CCR data.

GPR and CCR is, therefore, more appropriate for comprehensive geophysical architectural analysis.

In this case study, the geomorphology of a bar platform and channel scar suggest a laterally migrating channel bend, consistent with the classic meander model. However, the geophysical surveys in conjunction with direct subsurface observations indicate vertical accretion of gravel sheets is the dominant depositional process on the bar platform, an architecture associated with braided and wandering fluvial styles. Lateral migration is restricted to the outer, mid to downstream section of the platform, likely initiated after the bar emerged and the channel established. This study reiterates cautions raised by Brierley and Hickin (1991) that depositional process, and therefore architecture, may not always be functions of planform and that one may not be used to predict the other.

REFERENCES

ALLEN, J.R.L., 1963, The classification of cross-stratified units, with notes on their origin: Sedimentology, v. 2, p. 93–114.

ALLEN, J.R.L., 1983, Studies in fluviatile sedimentation: bars, bar complexes and sandstone sheets (low-sinuosity braided streams) in the Browstones (L. Devonian), Welsh borders: Sedimentary Geology, v. 33, p. 237–293.

ARCHIE, G.E., 1942, The electrical resistivity log as an aid in determining some reservoir characteristics: Transactions of the American Institute of Mining, Metallurgical, and Petroleum Engineers, v. 146, p. 54–67.

ASHMORE, P.E., 1991, How do gravel-bed rivers braid?: Canadian Journal of Earth Sciences, v. 28, p. 326–341.

BERES, M., AND HAENI, F.P., 1991, Application of ground-penetrating-radar methods in hydrogeologic studies: Ground Water, v. 29, p. 375–386.

BERES, M., GREEN, A., HUGGENBERGER, P., AND HORSTMEYER, H., 1995, Mapping the architecture of glaciofluvial sediments with 3-D Georadar: Geology, v. 23, p. 1087–1090.

BERES, M., HUGGENBERGER, P., GREEN, A., AND HORSTMEYER, H., 1999, Using two- and three-dimensional georadar methods to characterize glaciofluvial architecture: Sedimentary Geology, v. 129, p. 1–24.

BERSEZIO, R., GIUDICI, M., AND MELE, M., 2007, Combining sedimentology and geophysical data for high-resolution 3-D mapping of fluvial architectural elements in the Quaternary Po plain (Italy): Sedimentary Geology, v. 202, p. 230–248.

BEST, M.E., LEVSON, V.M., AND MCCONNELL, D., 2005, Sand and gravel mapping in Northeast British Columbia using airborne electromagnetic surveying methods, in Summary of Activities 2004, British Columbia Ministry of Energy and Mines, p. 1–6.

BEST, M.E., FERBEY, T., LEVSON, V.M., AND MCCONNELL, D., 2006, Airborne electromagnetic mapping for buried Quaternary sands and gravels in Northeast British Columbia, Canada: Journal of Environmental & Engineering Geophysics, v. 11, p. 17–26.

BRIDGE, J.S., 1985, Paleochannel patterns inferred from alluvial deposits: a critical evaluation: Journal of Sedimentary Petrology, v. 55, p. 579–589.

BRIDGE, J.S., AND MACKEY, S.D., 1993, A revised alluvial stratigraphy model, in Marzo, M., and Puigdefabregas, C., eds., Alluvial Sedimentation, International Association of Sedimentologists Special Publication 17, p. 319–336.

BRIDGE, J.S., ALEXANDER, J., COLLIER, R.E.L., GAWTHORPE, R.L., AND JARVIS, J., 1995, Ground-penetrating radar and coring used to study the large-scale structure of point-bar deposits in three dimensions: Sedimentology, v. 42, p. 839–852.

BRIDGE, J.S., COLLIER, R.E.L., AND ALEXANDER, J., 1998, Large-scale structure of Calamus River deposits (Nebraska, USA) revealed using ground-penetrating radar: Sedimentology, v. 45, p. 977–986.

BRIERLEY, G.J., 1989, River planform facies models: the sedimentology of braided, wandering, and meandering reaches of the Squamish River, British Columbia: Sedimentary Geology, v. 61, p. 17–35.

BRIERLEY, G.J., 1991, Bar sedimentology of the Squamish River, British Columbia: Definition and application of morphostratigraphic units: Journal of Sedimentary Petrology, v. 61, p. 211–225.

BRIERLEY, G.J., AND HICKIN, E.J., 1991, Channel planform as a non-controlling factor in fluvial sedimentology: The case of the Squamish River floodplain, British Columbia: Sedimentary Geology, v. 75, p. 67–83.

BRIERLEY, G.J., AND HICKIN, E.J., 1992, Floodplain development based on selective preservation of sediments, Squamish River, British Columbia: Geomorphology, v. 4, p. 381–391.

BRISTOW, C.S., 1993, Sedimentary structures exposed in bar tops in the Brahmaputra River, Bangladesh, in Best, J.L., and Bristow, C.S., eds., Braided Rivers, Geological Society of London, Special Publication 75, p. 277–289.

BRISTOW, C.S., 1995, Facies analysis in the Lower Greensand using ground-penetrating radar: Geological Society of London, Journal, v. 152, p. 591–598.

CARSON, M.A., 1984a, The meandering-braided river threshold: a reappraisal: Journal of Hydrology, v. 73, p. 315–334.

CARSON, M.A., 1984b, Observations on the meandering-braided river transition, the Canterbury Plains, New Zealand: New Zealand Geographer, v. 40, p. 12–17.

CARSON, M.A., 1984c, Observations on the meandering-braided river transition, the Canterbury Plains, New Zealand: New Zealand Geographer, v. 40, p. 89–99.

CHURCH, M.A., 1983, Pattern of instability in a wandering, gravel-bed channel, in Collinson, J.D., and Lewin, J., eds., Modern and Ancient Fluvial Systems, International Association of Sedimentologists, Special Publication 6, p. 169–180.

CLAERBOUT, J.F., AND MUIR, F., 1973, Robust modeling with erratic data: Geophysics, v. 38, p. 826–844.

DAVIS, J.L., AND ANNAN, A.P., 1989, Ground-penetrating radar for high resolution mapping of soil and rock stratigraphy: Geophysical Prospecting, v. 37, p. 531–551.

DEGROOT-HEDLIN, C., AND CONSTABLE, S., 1990, Occam's inversion to generate smooth, two-dimensional models from magnetotelluric data: Geophysics, v. 55, p. 1613–1624.

DESLOGES, J.R., AND CHURCH, M.A., 1987, Channel and floodplain facies in a wandering gravel-bed river, *in* Ethridge, F.G., Flores, R.M., and Harvey, M.D., eds., Recent Developments in Fluvial Sedimentology, SEPM, Special Publication 39, p. 99–109.

EDWARDS, L.S., 1977, A modified pseudosection for resistivity and induced-polarization: Geophysics, v. 42, p. 1020–1036.

FERGUSON, R.I., AND WERRITTY, A., 1983, Bar development and channel changes in gravelly River Feshie, Scotland, *in* Collinson, J.D., and Lewin, J., eds., Modern and Ancient Fluvial Systems, International Association of Sedimentologists, Special Publication 6, p. 181–193.

GAWTHORPE, R.L., COLLIER, R.E.L., ALEXANDER, J., BRIDGE, J.S., AND LEEDER, M.R., 1993, Ground penetrating radar: application to sandbody geometry and heterogeneity studies, *in* North, C.P., and Prosser, D.J., eds., Characterization of Fluvial and Aeolian Reservoirs, Geological Society of London, Special Publication 73, p. 421–432.

Geometrics Inc., 2001, OhmMapper TR1 Operation Manual: Geometrics Inc: San Jose, California, 147 p.

Geotomo Software, 2006, RES2DINV Rapid 2D Resistivity and IP Inversion: Geoelectrical Imaging 2D and 3D, Terraplus Inc.: Richmond Hill, Ontario, 132 p.

Golden Software, 2006, Voxler 3D Data Visualization: Golden Software Inc.: Golden, Colorado, 52 p.

GRIFFITHS, D.H., AND BARKER, R.D., 1993, Two-dimensional resistivity imaging and modelling in areas of complex geology: Journal of Applied Geophysics, v. 29, p. 211–226.

HUGGENBERGER, P., 1993, Radar facies: recognition of facies patterns and heterogeneities within Pleistocene Rhine gravels, NE Switzerland, *in* Best, J.L., and Bristow, C.S., eds., Braided Rivers, Geological Society of London, Special Publication 75, p. 163–176.

JOL, H.M., AND SMITH, D.G., 1991, Ground penetrating radar of northern lacustrine deltas: Canadian Journal of Earth Sciences, v. 28, p. 1939–1947.

KOSTIC, B., AND AIGNER, T., 2007, Sedimentary architecture and 3D ground-penetrating radar analysis of gravelly meandering river deposits (Neckar Valley, SW Germany): Sedimentology, v. 54, p. 789–808.

LECLERC, R.F., AND HICKIN, E.J., 1997, The internal structure of scrolled floodplain deposits based on ground-penetrating radar, North Thompson River, British Columbia: Geomorphology, v. 21, p. 17–38.

LOKE, M.H., AND BARKER, R.D., 1996, Rapid least-squares inversion of apparent resistivity pseudosections by a quasi-Newton method: Geophysical Prospecting, v. 44, p. 131–152.

MACKIN, J.H., 1937, Erosional history of Big Horn Basin, Wyoming: Geological Society of America, Bulletin, v. 48, p. 813–894.

MIALL, A.D., ed., 1978, Fluvial Sedimentology, Canadian Society of Petroleum Geologists, Memoir 5, 858 p.

MIALL, A.D., 1985, Architectural-element analysis: a new method of facies analysis applied to fluvial deposits: Earth-Science Reviews, v. 22, p. 261–308.

MIALL, A.D., 1994, Reconstructing fluvial macroform architecture from two-dimensional outcrops: examples from the Castlegate Sandstone, Book Cliffs, Utah: Journal of Sedimentary Research, v. 64, p. 146–158.

MIALL, A.D., 1996. The Geology of Fluvial Deposits; Sedimentary Facies, Basin Analysis and Petroleum Geology: Berlin, Springer-Verlag, 582 p.

MITCHUM, R.M., JR, VAIL, P.R., AND SANGREE, J.B., 1977, Seismic stratigraphy and global changes of sea level, part 6: stratigraphic interpretation of seismic reflection patterns in depositional sequences, *in* Payton, C.E., ed., Seismic Stratigraphy—Applications to Hydrocarbon Exploration, American Association of Petroleum Geologists, Memoir 26, p. 117–133.

MOYSEY, S., KNIGHT, R.J., AND JOL, H.M., 2006, Texture-based classification of ground-penetrating radar images: Geophysics, v. 71, p. 111–118.

MUMPY, A.J., JOL, H.M., KEAN, W.F., AND ISBELL, J.L., 2007, Architecture and sedimentology of an active braid bar in the Wisconsin River based on 3-D ground penetrating radar, *in* Baker, G.S., and Jol, H.M., eds., Stratigraphic Analysis using GPR, Geological Society of America, Special Paper 432, p. 111–131.

NANSON, G.C., AND KNIGHTON, A.D., 1996, Anabranching rivers: their cause, character and classification: Earth Surface Process and Landforms, v. 21, p. 217–239.

NEAL, A., 2004, Ground-penetrating radar and its use in sedimentology: principles, problems and progress: Earth-Science Reviews, v. 66, p. 261–330.

OLSEN, H., AND ANDREASEN, F., 1995, Sedimentology and ground-penetrating radar characteristics of a Pleistocene sandur deposit: Sedimentary Geology, v. 99, p. 1–15.

PALACKY, G.J., AND STEVENS, L.E., 1990, Mapping of Quaternary sediments in northeastern Ontario using ground electromagnetic methods: Geophysics, v. 55, p. 1595–1604.

PASSMORE, D.G., AND MACKLIN, M.G., 2000, Late Holocene channel and floodplain development in a wandering gravel-bed river: The River South Tyne at Lambley, Northern England: Earth Surface Processes and Landforms, v. 25, p. 1237–1256.

RAMSAY, J.G., 1967. Folding and Fracturing of Rocks: New York, McGraw-Hill, 568 p.

REYNOLDS, J.M., 1987, The role of surface geophysics in the assessment of regional groundwater potential in northern Nigeria, *in* Culshaw, M.G., Bell, F.G., Cripps, J.C., and O'Hara, M., eds., Planning and Engineering Geology, Geological Society of London, Engineering Group, Special Publication 4, p. 185–190.

REYNOLDS, J.M., 1997. An Introduction to Applied and Environmental Geophysics: New York, John Wiley & Sons, 796 p.

ROBERTS, M.C., BRAVARD, J.P., AND JOL, H.M., 1997, Radar signatures and structure of an avulsed channel: Rhône River, Aoste, France: Journal of Quaternary Science, v. 12, p. 35–42.

SCHUMM, S.A., 1985, Patterns of alluvial rivers: Annual Review of Earth and Planetary Sciences, v. 13, p. 5–27.

Sensors & Software, 1996, PulseEKKO IV User's Guide: Sensors & Software Inc.: Mississauga, Ontario, 59 p.

SMITH, N.D., 1974, Sedimentology and bar formation in the upper Kicking Horse River, a braided outwash stream: Journal of Geology, v. 82, p. 205–223.

STEPHENS, M., 1994, Architectural element analysis within the Kayenta Formation (Lower Jurassic) using ground-probing radar and sedimentological profiling, southwestern Colorado: Sedimentary Geology, v. 90, p. 179–211.

VANDENBERGHE, J., AND VAN OVERMEEREN, R.A., 1999, Ground penetrating radar images of selected fluvial deposits in the Netherlands: Sedimentary Geology, v. 128, p. 245–270.

WALKER, R.G., ed., 1979, Facies Models, Geological Association of Canada, Geoscience Canada, Reprint Series 1, 211 p.

WHITING, P.J., DIETRICH, W.E., LEOPOLD, L.B., DRAKE, T.G., AND SHREVE, R.L., 1988, Bedload sheets in heterogeneous sediments: Geology, v. 16, p. 105–108.

WILLIS, B.J., 1989, Paleochannel reconstruction from point bar deposits: a three-dimensional perspective: Sedimentology, v. 36, p. 757–766.

WOODWARD, J., ASHWORTH, P.J., BEST, J.L., SAMBROOK SMITH, G.H., AND SIMPSON, C.J., 2003, The use and application of GPR in sandy fluvial environments: methodological considerations, *in* Bristow, C.S., and Jol, H.M., eds., Ground Penetrating Radar in Sediments, Geological Society of London, Special Publication 211, p. 127–142.

WOOLDRIDGE, C.L., AND HICKIN, E.J., 2005, Radar architecture and evolution of channel bars in wandering gravel-bed rivers: Fraser and Squamish rivers, British Columbia, Canada: Journal of Sedimentary Research, v. 75, p. 844–860.

WRIGHT, M.D., 1959, The formation of cross-bedding by a meandering or braided stream: Journal of Sedimentary Petrology, v. 29, p. 610–615.